



HAL
open science

The Arches cluster revisited

J. S Clark, M. E Lohr, F. Najarro, H. Dong, F. Martins

► **To cite this version:**

J. S Clark, M. E Lohr, F. Najarro, H. Dong, F. Martins. The Arches cluster revisited. *Astronomy and Astrophysics - A&A*, 2018, 617, pp.A65. 10.1051/0004-6361/201832826 . hal-01992794

HAL Id: hal-01992794

<https://hal.science/hal-01992794>

Submitted on 24 Jan 2019

HAL is a multi-disciplinary open access archive for the deposit and dissemination of scientific research documents, whether they are published or not. The documents may come from teaching and research institutions in France or abroad, or from public or private research centers.

L'archive ouverte pluridisciplinaire **HAL**, est destinée au dépôt et à la diffusion de documents scientifiques de niveau recherche, publiés ou non, émanant des établissements d'enseignement et de recherche français ou étrangers, des laboratoires publics ou privés.

The Arches cluster revisited

I. Data presentation and stellar census[★]

J. S. Clark¹, M. E. Lohr¹, F. Najarro², H. Dong³, and F. Martins⁴

¹ School of Physical Sciences, The Open University, Walton Hall, Milton Keynes MK7 6AA, UK
e-mail: s.clark@open.ac.uk

² Departamento de Astrofísica, Centro de Astrobiología, (CSIC-INTA), Ctra Torrejón a Ajalvir, km 4, 28850 Torrejón de Ardoz, Madrid, Spain

³ Instituto de Astrofísica de Andalucía (CSIC), Glorieta de la Astronomía s/n, 18008 Granada, Spain

⁴ LUPM, Université de Montpellier, CNRS, Place Eugène Bataillon, 34095 Montpellier, France

Received 13 February 2018 / Accepted 23 March 2018

ABSTRACT

Context. Located within the central region of the Galaxy, the Arches cluster appears to be one of the youngest, densest, and most massive stellar aggregates within the Milky Way. As such, it has the potential to be uniquely instructive laboratory for the study of star formation in extreme environments and the physics of very massive stars.

Aims. To realise this possibility, the fundamental physical properties of both cluster and constituent stars need to be robustly determined; tasks we attempt here.

Methods. In order to accomplish these goals we provide and analyse new multi-epoch near-IR spectroscopic data obtained with the VLT/SINFONI and photometry from the HST/WFC3. We are able to stack multiple epochs of spectroscopy for individual stars in order to obtain the deepest view of the cluster members ever obtained.

Results. We present spectral classifications for 88 cluster members, all of which are WNLh or O stars: a factor of three increase over previous studies. We find no further examples of Wolf–Rayet stars within the cluster; importantly no H-free examples were identified. The smooth and continuous progression in spectral morphologies from O super/hypergiants through to the WNLh cohort implies a direct evolutionary connection. We identify candidate giant and main sequence O stars spectroscopically for the first time. No products of binary evolution may be unambiguously identified despite the presence of massive binaries within the Arches.

Conclusions. Notwithstanding difficulties imposed by the highly uncertain (differential) reddening to the Arches, we infer a main sequence/luminosity class V turn-off mass of $\sim 30\text{--}38 M_{\odot}$ via the distribution of spectral types. Analysis of the eclipsing binary F2 suggests current masses of $\sim 80 M_{\odot}$ and $\sim 60 M_{\odot}$ for the WNLh and O hypergiant cohorts, respectively; we conclude that all classified stars have masses $> 20 M_{\odot}$. An age of $\sim 2.0\text{--}3.3$ Myr is suggested by the turn-off between $\sim O4\text{--}5$ V; constraints imposed by the supergiant population and the lack of H-free WRs are consistent with this estimate. While the absence of highly evolved WC stars strongly argues against the prior occurrence of SNe within the Arches, the derived age does accommodate such events for exceptionally massive stars. Further progress will require quantitative analysis of multiple individual cluster members in addition to further spectroscopic observations to better constrain the binary and main sequence populations; nevertheless it is abundantly clear that the Arches offers an unprecedented insight into the formation, evolution and death of the most massive stars nature allows to form.

Key words. stars: early-type – stars: evolution – stars: Wolf–Rayet – open clusters and associations: general – Galaxy: nucleus – open clusters and associations: individual: Arches cluster

1. Introduction

Determining the formation mechanism, properties and lifecycle of very massive stars is one of the most important unresolved issues in stellar astrophysics; a problem exacerbated by their impact on galactic evolution – via radiative, mechanical, and chemical feedback – and their role as progenitors of some of the most luminous electromagnetic and gravitational wave transients in the Universe. Currently, even the most basic questions – such as how massive nature permits stars to grow – remain unanswered. How do they reach their final masses – do they form via a scaled up version of the disc-mediated accretion paradigm

for low mass stars (Shu et al. 1987), competitive accretion in a clustered environment (Bonnell et al. 2001) or are they instead built-up by a more exotic avenue such as mergers, either before or during core-H burning (Schneider et al. 2014, 2015)? Competitive accretion suggest that massive stars should form in stellar aggregates (clusters or OB associations) but is this always the case? And a related question – does the environment in which they form influence their final properties, such as occurrence of binarity and the form of the initial mass function (IMF)?

The central regions of our Galaxy provide a unique laboratory for the study of massive stars, hosting 3 young (< 10 Myr), massive ($\geq 10^4 M_{\odot}$) clusters; the Galactic centre, Quintuplet and the Arches. Critically, their co-location and consequently well defined distance aids luminosity determinations for cluster members; observationally challenging for isolated field stars in the galactic disc. Moreover the cluster ages they span means

[★] Based on observations made at the European Southern Observatory, Paranal, Chile under programmes ESO 087.D-0317, 091.D-0187, and 099.D-0345.

that evolutionary pathways for a wide range of initial masses ($\sim 20\text{--}100 M_{\odot}$) may be constrained via study of their evolved stellar populations.

We may also invert this argument, utilising these clusters to explore the effects of the extreme Galactic centre environment on (massive) star formation and the role their subsequent feedback plays in the wider ecology of the circumnuclear molecular and starburst region. In this respect the proximity of the Galactic centre renders it the sole testbed for studying the physics, recent star formation history and assemblage of the circumnuclear starburst of a galaxy at the level of individual constituent stars.

Of the three circumnuclear clusters, the Arches (Cotera et al. 1996) is of particular interest, given its (i) apparent youth and high mass – resulting in the upper reaches of the IMF being well populated – and (ii) compactness – leading to an extreme stellar density (Figer et al. 1999b; Martins et al. 2008, henceforth Ma08). Consequently numerous studies of the Arches have been undertaken in the two decades following its discovery to better understand its bulk properties and those of its constituent stars. The majority of these have focused on determining the shape of the IMF and the presence of possible mass segregation, although such efforts are hampered by uncertainties in the extinction law and significant differential reddening across the field (Figer et al. 2002, henceforth Fi02; Stolte et al. 2002, 2005; Kim et al. 2006; Espinoza et al. 2009; Clarkson et al. 2012; and Habibi et al. 2013).

Corresponding spectroscopic observations to classify and date the constituent stars and cluster are more limited (Fi02, Najarro et al. 2004, Ma08) but reveal homogeneous populations of highly luminous WN7-9h and mid-O supergiants, with two mid-O hypergiants with spectral morphologies intermediate between these groups. Assuming uniform reddening, non-LTE model-atmosphere analysis of these stars by Ma08 suggested that stars in both cohorts are very massive ($>60 M_{\odot}$) and young, with a global age of 2–4 Myr suggested for the Arches. Intriguingly, at the lower extent of the age-range no supernovae (SNe) would be expected to have occurred and hence the most massive stars born within the Arches should still be present ($\geq 100 M_{\odot}$; Crowther et al. 2010), allowing us to probe the upper reaches of the IMF and the stars that populate it. Moreover, the modelling results also hint at non-coevality for the cluster, with the more luminous WN7-9h stars potentially being younger than the less evolved supergiants.

Following the recognition of the prevalence and importance of binarity to understanding massive stellar evolution (Sana et al. 2012; de Mink et al. 2014), Schneider et al. (2014) re-interpreted the cluster (I)MF and age of the Arches under the assumption that all the massive stars within were binaries. As a result they revised the cluster age to a unique value of 3.5 ± 0.7 Myr, and concluded that the brightest 9.2 ± 3 stars (all WN7-9h) were the rejuvenated products of binary interaction – essentially indicating that very massive stars could form via a two-stage process with a second episode of mass-accretion onto the secondary during the H-burning phase of the primary.

Given the extreme requirements placed on the binary population of the Arches by Schneider et al. (2014) in order to explain the apparent non-coevality of the Arches (cf. Ma08), improved observational constraints on the cluster properties are imperative. Moreover, due to the anticipated youth of the Arches, such studies would also provide important insights into the formation and lifecycle of extremely massive stars. Unfortunately, no systematic survey for binarity within the Arches has yet been attempted, although indirect diagnostics suggest binarity for a number of cluster members (e.g. Wang et al. 2006). A better

determination of the cluster age would also require improved bolometric luminosity estimates – via individually determined corrections for interstellar reddening (Sect. 4) – to facilitate improved isochrone fitting, in conjunction with the identification of the main sequence turn-off.

In order to address these issue we undertook a multi-epoch spectroscopic survey of the Arches with the integral field spectrograph SINFONI mounted on the Very Large Telescope (VLT). These observations permitted a search for both radial velocity and line profile variability, potentially indicative of reflex binary motion and wind collision zones, respectively. Moreover, stacking multiple individual observations allowed us to obtain higher signal/noise (S/N) spectra and hence reach less evolved cluster members than previous studies. These data were supplemented with new *Hubble* Space Telescope (HST) Wide Field Camera 3 (WFC3) photometry. In this work we present the resultant datasets and utilise them to provide an updated stellar census of the Arches and discuss the impact of the new data on the determination of cluster properties. Companion papers provide a tailored quantitative analysis of the binary system F2 (adopting the naming convention of Fi02) and discuss the spectral variability of cluster members (Lohr et al. 2018 and Lohr et al. in prep.; henceforth Papers II and III).

This paper is structured as follows. In Sect. 2 we present the data acquisition and reduction strategies employed. In Sect. 3 we provide spectral classifications for cluster members, which are summarised in Table A.1. The important and complicating issue of interstellar extinction towards the Arches is investigated in Sect. 4, while in Sect. 5 we address the implications of our new results for the stellar masses of the cluster members and the determination of the cluster age. Finally we discuss evolutionary implications in Sect. 6 and in Sect. 7 summarise our findings and highlight future prospects.

2. Data acquisition and reduction

2.1. Spectroscopy

As initially envisaged, our programme was to closely follow the observational strategy of Ma08. Specifically, between April and August 2011 the SINFONI integral field spectrograph on the ESO/VLT (Eisenhauer et al. 2003; Bonnet et al. 2004) was used in service mode to make multiple K band observations of three overlapping fields in the central Arches cluster, and seven fields on the periphery of the cluster. For each observation four 60 s exposures nodding across the target field were taken, interspersed with sky frames to optimise background removal for the combined images. Telluric standards with spectral types B2–B9 were observed before or after each set of science frames.

However poor weather significantly impacted on observations, leaving the programme substantially unfinished. As a consequence further time was sought and awarded, with observations made from March to August 2013 and again from April to July 2017. Unfortunately, on each occasion the programmes remained incomplete at the end of the semester. This resulted in a highly inhomogeneous composite dataset, with some fields visited multiple times, while other outliers were only observed once or twice. Moreover, the signal-to-noise (S/N) of individual integrations was highly variable given the poor observing conditions in which some observations were attempted. In order to generate the most complete dataset possible, previous spectroscopic observations of the Arches utilising the same experimental set-up were extracted from the archive¹, to be reduced in an

¹ ESO proposals O87.D-0342 and 093.D-0306.

identical manner (see below). A further epoch of spectroscopy covering outlying fields was extracted from data cubes used for Ma08²; in this instance sky subtraction and telluric removal was carried out via the methodology described in that paper.

A detailed breakdown of the timings of individual observations is provided in Paper III and we refer the interested reader to this work. Foreshadowing the following discussion, since we are only interested in obtaining the highest quality summed spectra for this work we simply list the number of individual, contributing observations for each cluster member in Table A.1. In a number of cases multiple individual observations were made on the same night – hence we also list the total number of nights (epochs) on which data were obtained.

Science and telluric standard frames were reduced with the latest version of the ESO SINFONI pipeline running under Reflex. This performed flat-fielding and optical distortion corrections, wavelength calibration and improved sky background subtraction, before stacking slitlets into data cubes for each frame, and co-adding cubes for each subfield and for each observation. QFitsView was initially used to inspect the reduced cubes³, and then a custom IDL code was written to facilitate manual extraction of spectra for multiple individual pixels associated with each science target or telluric standard star. Care had to be taken to avoid selection of pixels contaminated by light from nearby objects; on certain epochs, unwanted instrumental features were observable in specific regions of the data cube, so these pixels were also excluded.

These pixel-spectra were then combined into a single spectrum per object, using an approach based on the optimal extraction algorithm for long-slit spectra of Horne (1986). Specifically, spatial profiles were determined for each pixel-spectrum (indicating the probability that a detected photon at a given wavelength would be registered in that pixel) by dividing the pixel’s flux at each wavelength by the total flux over all pixels at that wavelength, and then median-smoothing the resulting profile estimates to reduce the impact of bad lines in individual pixels. Each pixel’s fluxes were then divided by its smoothed spatial profile to give an estimate of the total spectrum; the median of all such estimates was then taken as our best estimate of the object’s one-dimensional spectrum.

Preliminary radial velocity measurements indicated small but significant errors in the wavelength solutions obtained by the pipeline software. Therefore, corrections were determined by cross-correlating all science and telluric spectra with a standard high resolution telluric spectrum in the *K* band provided by ESO⁴, using the IRAF telluric task, and the headers adjusted accordingly.

The only intrinsic absorption line in our telluric spectra, in the wavelength region of interest, was the Bry line at 2.166 μm . This was removed by fitting it with a double Lorentzian profile. When two telluric standards had been observed in a given epoch, before and after a set of science frames, a custom telluric spectrum was created for each science observation by interpolating between the two standards, to match the time of the science observation, and normalising to the continuum. Each science spectrum was then divided by the appropriate telluric spectrum with the aid of a custom code; this determined optimal scalings of small regions of the telluric spectrum to match the corresponding telluric lines in the science spectrum, and then fitted

these with a smoothly-varying function to give optimal scalings at every wavelength for the telluric spectrum. The telluric-removed science spectra were then normalised to the continuum.

Where multiple observations had been made of a science target within the same epoch (in practice, within a few hours of each other on the same night) they had barycentric corrections applied, and were then median-combined. A search for radial velocity variability between epochs in the brighter cluster members, described fully in Paper III, was then carried out, and where variability was detected, all epochs were shifted to a common velocity (the mid-point of the full range of measured velocities), and then median-combined. Fainter stars, and those which were only observed on a single epoch, or for which radial velocity variability could not be reliably measured, were directly median-combined. All final combined spectra were checked, and occasional residual bad features manually removed.

SINFONI provides a resolving power (in the *K*-band and at our plate scales of 0'1 or 0'025) of $R \sim 4500$ at 2.2 μm . All spectra were rebinned to a common dispersion of 0.000245 $\mu\text{m pixel}^{-1}$ and common wavelength range of 2.02–2.45 μm .

In total we extracted spectra for 105 objects. Excluding four apparent late-spectral type interlopers we present the resultant spectra of all cluster members in Fig. A.1, where, following Fi02, they are ordered by decreasing estimated absolute *K*-band magnitude. Of these 88 appear to be both cluster members and of suitable S/N to attempt classification (Sect. 3), more than tripling the spectroscopic sample presented by Ma08 and critically extending the census to lower luminosity objects. Representative spectra illustrating each spectral type and/or luminosity class are presented in Figs. 1–6.

2.2. Photometry

Despite the availability of ground-based AO observations, we have chosen to exclusively employ HST data due to its high angular resolution and sensitivity, stability of point spread function and accurate zeropoint; invaluable given the compact nature of the Arches. As well as employing photometry from Fi02 (F110W, F160W, and F205W) and (Dong et al. 2011; NIC3 F190N) we present new WFC3 photometry in the F127M, F139M, and F153M filters. The relevant data were obtained in 2010–12 under programmes GO-11671, 12318, and 12667 (PI Andrea Ghez). A detailed description of data acquisition, reduction and analysis, including error determination, is presented by Dong et al. (2017), which, for convenience, we reprise here.

Raw data and calibration files were downloaded and the latest HST pipeline, OPUS version and CAL-WFC3 version 2.1 were used to perform basic calibration steps on individual dithered exposures such as bias correction and flat fielding. Under PyRAF the “Tweakier” and “Astrodizzle” tasks aligned individual exposures and corrected for distortion and masking out defects before combining images.

The “DOLPHOT” package⁵ (Dolphin 2000) was employed to extract photometry. DOLPHOT returns photometric uncertainty resulting from Poisson fluctuations produced by electrons in the camera and also allowed us to perform additional artificial star tests on the dithered images to provide a secondary, parallel error determination. For each star we used the larger resulting error estimate. We present error estimates as a function of magnitude for each filter in Fig. 7; with the exception of a handful of examples these are less than ~ 0.05 mag in each band.

² ESO proposal 075.D-0736.

³ <http://www.mpe.mpg.de/~ott/QFitsView/>

⁴ https://www.eso.org/sci/facilities/paranal/decommissioned/isaac/tools/spectra/atmos_S_K.fits

⁵ <http://americano.dolphinim.com/dolphot/>

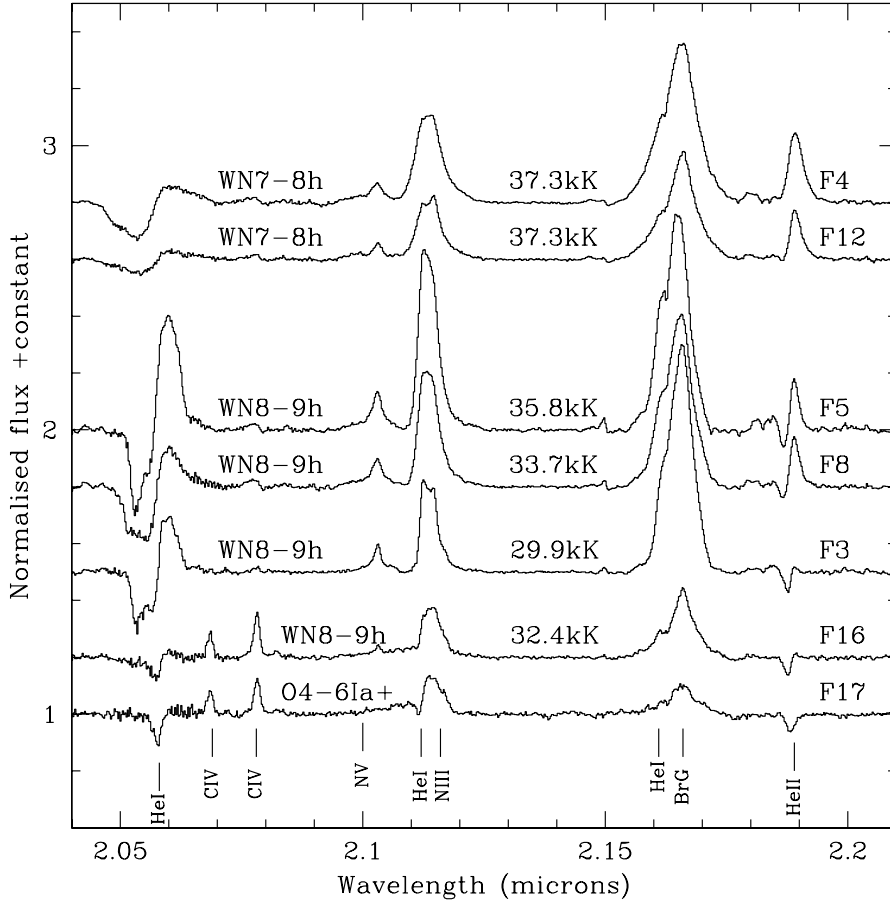


Fig. 1. *K*-band spectra of selected WRs ordered on the basis of the morphology of the He II 2.189 μm line. Spectral types and temperatures inferred by Ma08 indicated. The spectrum of F17, which appears intermediate between the O4-6 Ia⁺ stars and the least extreme WN8-9h star, F16, is shown for comparison.

The resultant photometry, along with the pseudo *K*-band F205W magnitudes from Fi02 are presented in Table A.1.

3. Spectral classification

Our observations sample stars with *K*-band (F205W) magnitudes ranging from ~ 10.4 (F6) through to ~ 14.5 (F155) and ~ 15 (F188). Foreshadowing the discussion of interstellar extinction in Sect. 4, Fi02 estimate these correspond to $M_K \sim -8$ to -3.1 . In total we extracted spectra of 105 individual stars. Of these, spectra of four stars⁶ showed pronounced CO bandhead absorption, marking them as M star interlopers. The spectra of a further five stars⁷ may potentially be contaminated by bright neighbours and hence are not considered further. A number of fainter objects⁸ were of sufficiently low S/N that accurate spectral classification was impossible. However, these are retained for the purpose of discussion since their essentially featureless spectra are not consistent with identification as e.g. evolved Wolf-Rayets, since the broad and strong emission lines expected for such objects would have been readily identifiable. Finally three further stars demonstrated essentially featureless spectra⁹ despite having a sufficient S/N to identify the classification diagnostics for e.g. main sequence stars if present. This left a total of 88 stars for which spectral classification could be attempted, to which we may also add the reconstructed spectrum of the secondary in the massive binary system F2 (Paper II).

⁶ F11, F46, F51, and F99.

⁷ F44, F73, F80, F166, and F170.

⁸ F159, F168, F173, F174, and F184.

⁹ F151, F176, and F189.

3.1. Classification criteria

A number of authors have studied the utility of near-IR spectroscopy for classification of early-type stars; specifically Hanson et al. (1996, 2005) and Crowther & Furness (2008) provide quantitative criteria for OB stars, with Crowther et al. (2006) and Rosslowe & Crowther (2018) replicating these efforts for WRs and Crowther & Walborn (2011) extending these studies to extremely luminous stars sharing properties of both classes. Drawing on these studies where available, Ma08 discuss and present classification criteria for stars within the Arches in some depth; for consistency we adopt their scheme for this study, revising their spectral types and/or luminosity class assignments only when suggested by the improved S/N of the data presented here.

However, the increased integration times afforded by stacking multiple spectra of individual objects results in qualitatively different spectral morphologies amongst the fainter Arches cohort. Consequently it is worth revisiting the classification criteria afforded by the *K*-band. Prime temperature diagnostics include the He II 2.189 μm line and the absorption line associated with the He I 2.112 μm component of the broad blend resulting from transitions of He I, N III, C III, and O III (cf. Hanson et al. 1996, 2005), with the C IV transitions between 2.07 and 2.08 μm providing a secondary criterion for stars between O4-8 (peaking at \sim O5 and decreasing either side).

An additional diagnostic for early-type stars that is not discussed in the above works is the strong emission feature at $\sim 2.42 \mu\text{m}$ that is, subject to sufficient S/N, ubiquitous for the vast majority of our spectra. Non-LTE model atmosphere simulations utilising the CMFGEN code (Hillier & Miller 1998, 1999) suggest the identity of this feature is sensitive to temperature, with contributions from, respectively, the $n = 10 \rightarrow 9$ 2.436–8 μm lines

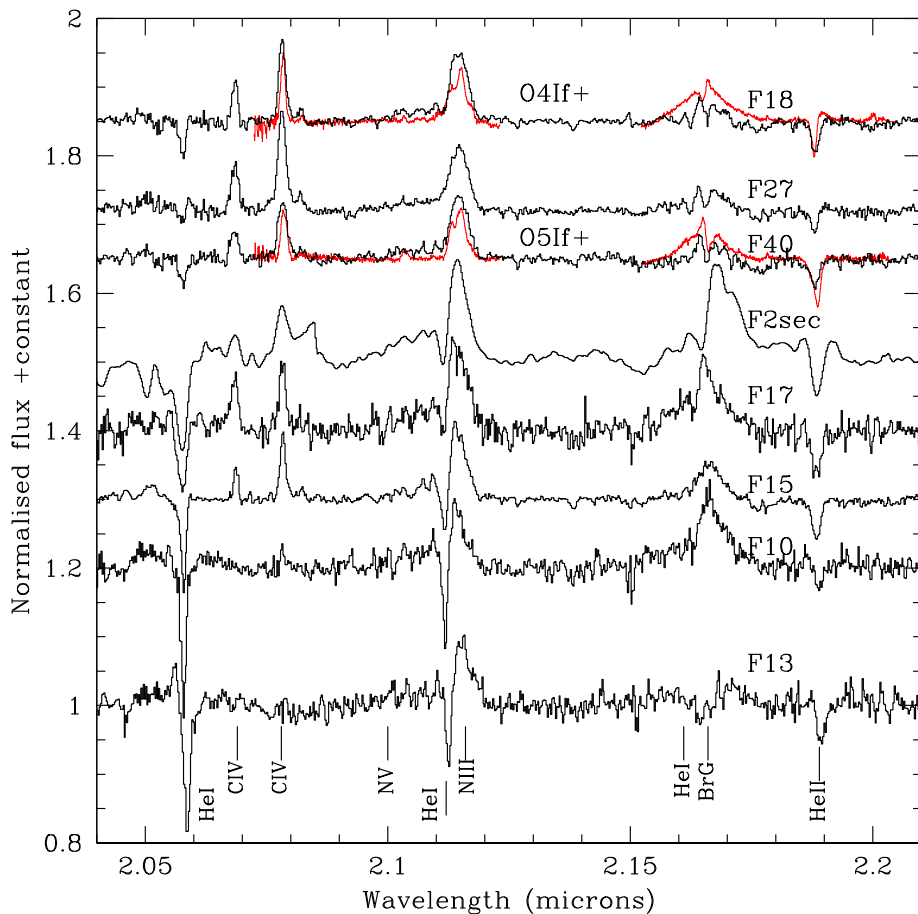


Fig. 2. *K*-band spectra of potential extreme O-type supergiant or hypergiant cluster members (black) compared to appropriate template spectra from Hanson et al. (2005; red).

of O IV, N IV, C IV, and finally Si IV as one transitions to cooler temperatures. Since the WNLh stars considered here are likely $>30\text{ kK}$ we would expect Si IV to dominate the emission feature. N IV starts to contribute at $\sim 32\text{ kK}$, equalling the strength of Si IV at 36.5 kK . Subject to depletion C IV might be expected to play a minor contribution; since these stars are almost certainly cooler than $\sim 45\text{ kK}$ one would not expect a contribution from the O IV. Similarly for supergiants of spectral type mid-O and later one would expect this feature to result from a combination of Si IV, C IV, and N IV, with Si IV increasingly dominant for cooler stars.

Bry is another key diagnostic line, providing valuable information on both the mass-loss rate and the luminosity class of the star via the observation that, in general, increased luminosity is associated with elevated mass-loss rates. Such a relationship appears realised in the Arches, where the line is seen fully in emission in both the WR and hypergiant cohorts. Less-evolved stars support lower stellar luminosities and are normally associated with reduced mass-loss rates, favouring a transition to photospheric absorption profiles and motivating the division between hypergiants and supergiants adopted by Ma08. Once seen in absorption, the shape of the photospheric profile may in theory be used to assign a luminosity class via the dependence on surface gravity (Hanson et al. 2005). However, given the luminosities of the stars in question in this study, this may be complicated by residual contamination of the profile by wind emission and rotational broadening (although the latter is typically dominated by the large intrinsic widths of the photospheric absorption wings).

Once the additional temperature dependence of the H I and He I transitions is taken into account it becomes difficult to

finely discriminate between adjacent luminosity classes (e.g. Ia, Ib and II and III–V). This is illustrated in Fig. 8, where we compare template spectra for giant and main sequence objects from Hanson et al. (2005). For mid-O (O5–6) spectral types the strength of C IV emission distinguishes between luminosity types, being systematically stronger in the giants. However despite the excellent S/N ratio (>100) of the spectra, once this diagnostic disappears at lower temperatures it becomes more problematic to reliably differentiate between $\sim\text{O7–O9}$ giant and main sequence stars, since in isolation one is forced to rely solely on the wings of the Bry photospheric line.

Nevertheless, for a subset of high S/N spectra – exemplified by F68, F77, and F96 (Fig. 4) – a classification as giant appears most appropriate given both the marked similarity to the spectroscopic standards of Hanson et al. (2005) and notable differences compared to the “bona fide” Arches supergiants (cf. discussion in Sect. 3.2). Likewise we may identify a number of candidate early-mid O dwarfs amongst the photometrically faintest cluster members – e.g. F87 and F112 (Fig. 5) – that differ from the assumed giant cohort due to the comparative weakness of C IV emission. Both sets of spectra may hence be employed as “anchor points” from which one may “bootstrap” classify other similar but lower S/N spectra and, in the case of the main sequence candidates, stars of later spectral type, which demonstrate a smooth morphological progression. A similar approach was also adopted for the more luminous super- and hypergiants within the Arches. We discuss this process in more detail below, cautioning that this still leaves a number of stars for which an indeterminate – e.g. I–III or III–V - luminosity class is most appropriate given the quality of the current dataset.

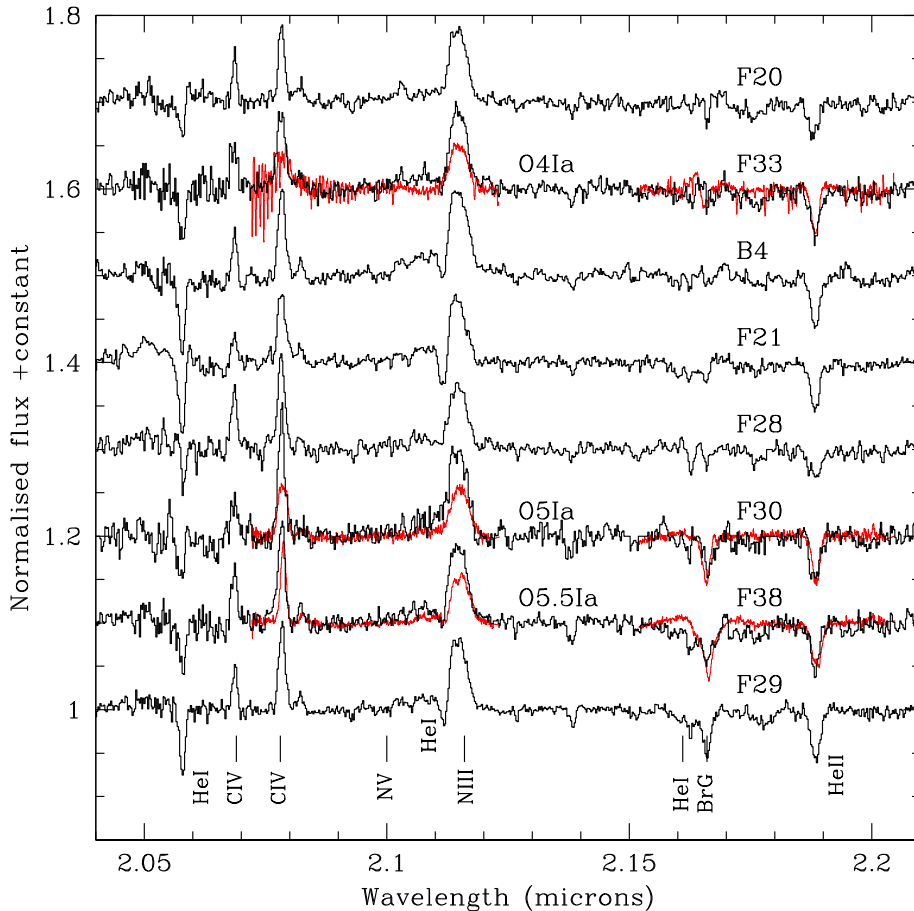


Fig. 3. *K*-band spectra of O supergiants within the Arches previously sampled by Ma08 (black) compared to template spectra from Hanson et al. (2005; red).

3.2. Analysis of the dataset

The principal conclusion from consideration of the whole dataset is that there is a remarkable similarity and continuity between the spectra of individual stars within the Arches as one progresses from higher to lower luminosity objects. While we are able to identify qualitatively distinct spectral morphologies amongst the fainter cluster members when compared to the more luminous subset presented by Ma08, the population of the Arches that we sample appears to consist predominantly, and possibly exclusively of WNLha and O stars. As described below, despite reaching a magnitude at which they should be detectable, we are unable to detect any more evolved Wolf-Rayets in the cluster, such as H-depleted WNE or WC stars. Likewise transitional objects such as luminous blue variables (LBV) and blue hypergiants of later spectral type are also absent. These findings have important consequences for the age of the Arches, which we return to in Sect. 5. We emphasise at this point that the spectral and luminosity classifications discussed below are based solely on spectroscopic data. Unfortunately, the absolute magnitudes of individual stars, which would aid classification, are dependent on the highly uncertain extinction law towards the Arches and the differential reddening evident across the cluster. Indeed it is hoped that identification of stars with a well defined luminosity, such as the main sequence, will help refine these parameters: an issue we return to in Sect. 4.

3.2.1. WRs and O-hypergiants

With Arches F11 identified as a foreground interloper, we fail to identify any further WRs within the Arches, while the higher

S/N spectra provide no compelling evidence to revisit their spectral classifications. A subset of spectra are plotted in Fig. 1 and following Crowther et al. (2006, 2010) are ordered primarily by the strength and morphology of the He II 2.189 μm line, the ratio of which to Br γ serves as a classification criterion for WNLh stars. As anticipated this broadly correlates with a decrease in the temperatures for individual stars found by Ma08. Considerable diversity is present in the spectral morphologies of these stars, most notably in the shape of the He I profile and the strengths of the nitrogen, carbon and oxygen transitions, which Ma08 attribute to differences in CNO burning products at the stellar surface.

Ma08 identify two extreme O super-/hypergiants – F10 and F15 – within the Arches on the basis of strong Br γ emission, a criterion also consistent with examples presented in the spectral atlas of Hanson et al. (2005). Following this criterion we significantly expand on the number of O hypergiants present in the cluster, identifying a further six candidates – the secondary in the binary F2, F13, F17, F18, F27, and F40 (Fig. 2).

We highlight the morphological similarities between the most extreme example, F17, and the least extreme WNLh within the cluster, F16, which suggest a close evolutionary connection between the two classes of star (Fig. 1). Indeed the increased population of hypergiants within the Arches strengthens the hypothesis by Ma08 that they represent an intermediate evolutionary phase between the supergiant and WR populations.

Of the hypergiants, comparison of F18, F27, and F40 to the template spectra of Hanson et al. (2005) suggest that they are O4-5 If⁺ stars, albeit with slightly lower mass-loss rates inferred from the weaker Br γ emission. Conversely the secondary in the eclipsing binary F2 along with F10, F15, and F17

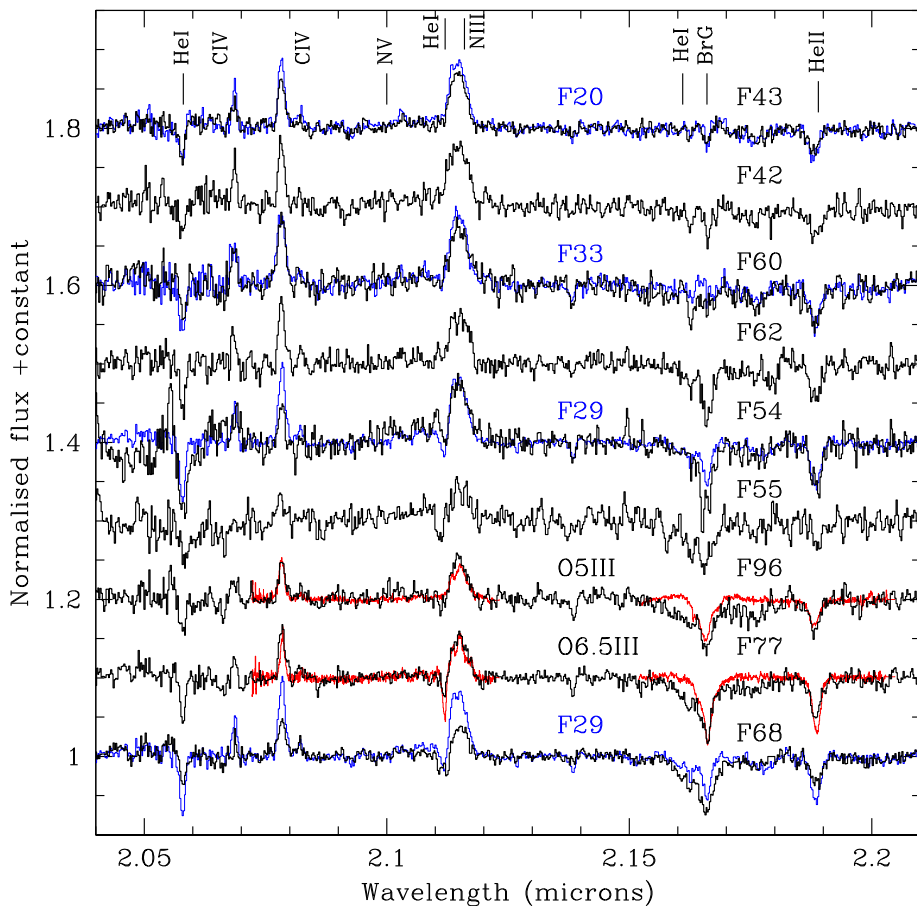


Fig. 4. Comparison of cluster members (black) to previously classified cluster supergiants (blue) and mid O giant template K -band spectra from [Hanson et al. \(2005\)](#); red). We note that no template spectra earlier than O5 III are available.

demonstrate much stronger Bry emission along with the presence of a notable absorption component to the $2.11\ \mu\text{m}$ blend attributable to the He I $2.112\ \mu\text{m}$ transition (behaviour mirrored in the He I $2.059\ \mu\text{m}$ singlet). In conjunction with the reduction in strength of the C IV $2.069\ \mu\text{m}$ and $2.079\ \mu\text{m}$ lines – the object with the deepest He I $2.112\ \mu\text{m}$ feature, F10, also shows the weakest C IV emission – this observation suggests these are cooler objects than F18, F27, and F40, albeit with denser winds. Given the lack of suitable spectral templates we provisionally classify these as O5-6 Ia⁺ (F2 secondary and F17), O6-7 Ia⁺ (F15), and O7-8 Ia⁺ (F10), noting that quantitative model-atmospheric analysis will be required to confirm this spread in temperatures.

Finally we turn to F13 which, despite sporting weak Bry absorption demonstrates deep absorption in the He I lines and a lack of C IV emission – a combination of features not replicated in any other cluster member with the exception of F10. Given this, and mindful of the Bry absorption we therefore adopt a similar classification of O7-8 Ia⁺.

3.2.2. O supergiants

Next we consider the O supergiants within the Arches, concentrating first on the brighter cohort considered by Ma08, comprising 13 stars between F18 and F40, to which we add a further six stars¹⁰, all of which appear to be O supergiants. Attribution of absolute spectral types is complicated by the lack of suitable template spectra, particularly for stars of the luminosities expected for the Arches. In this respect we highlight that comparison to the spectra of [Hanson et al. \(2005\)](#) reveals that

¹⁰ B4, F19, F24, F25, F30, and F38.

emission lines in cluster supergiants are systematically stronger (cf. F30 and F33; Fig. 3). Nevertheless the higher S/N afforded by the new data allows us to provide robust relative calibrations since we can now reliably identify systematic variations in both Bry (a proxy for mass-loss rate/wind density) and He I $2.112\ \mu\text{m}$ (temperature) lines (Fig. 3).

While the majority of these stars show the $2.11\ \mu\text{m}$ blend purely in emission, indicative of an O4-5 Ia classification (e.g., F20, F28, and F33; Figs. 3 and A.1 and Table A.1), five stars show He I $2.112\ \mu\text{m}$ absorption components of various strengths, suggestive of later spectral types; we assign provisional classifications of O5.5-6 Ia (B4, F22, and F29) and O6-6.5 Ia (F21 and F23). Irrespective of spectral type we identify varying degrees of infilling of the He I+Bry photospheric blend, which is almost absent in B4, F20, F21, and F33 (Figs. 3 and A.1). This would suggest a close connection with the hypergiants – where this blend is seen in emission – for these stars, with F20 and F33 (no He I $2.112\ \mu\text{m}$ absorption) being direct antecedents of hotter O hypergiants such as F18, F27, and F40, while B4 and F21 (He I $2.112\ \mu\text{m}$ absorption) fulfil this role for the cooler hypergiants F10, F15 and F17.

We now turn to fainter stars for which no previous spectra have been published; these would be expected to comprise lower luminosity supergiants, giants and possibly main sequence objects. We present a montage of spectra of selected stars in Fig. 4 and it is immediately clear from comparison to known supergiants that additional examples are present within this cohort - e.g. F42, F43, and F60. In total we identify a further 8 supergiants, noting that none have spectral types outside the previous range (O4-6.5 Ia; Table A.1). We caution that following Fi02, the increasing “F” numbers of these stars is indicative

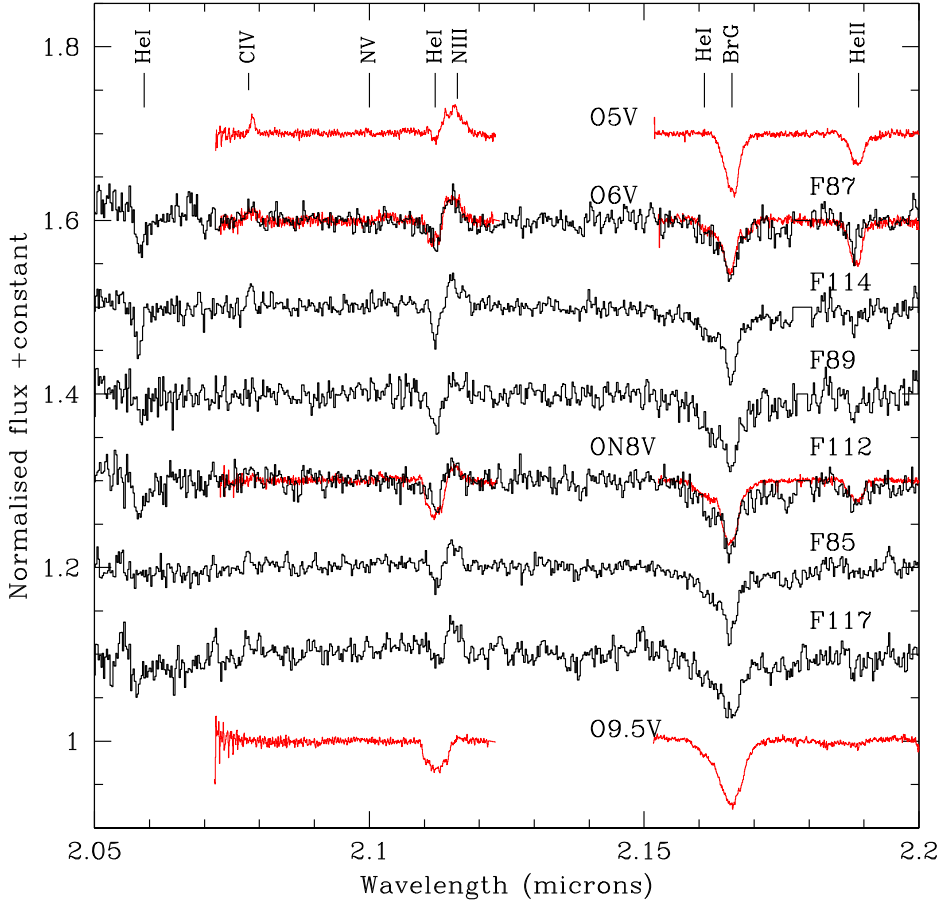


Fig. 5. Comparison of selected fainter cluster members (black) with MS K -band template spectra from Hanson et al. (2005; red).

of reduced luminosities and so luminosity classes Ia b, b, or II may in reality be more appropriate for some than the generic Ia assigned here. Indeed this possibility is reflected in the assignment of a luminosity class I–III for six stars for which emission lines are significantly weaker than “bona fide” supergiants (cf. F54 and F62 in Fig. 4, Table A.1).

To summarise: Ma08 identified 13 mid-O supergiants of which we reclassify two as hypergiants. We more than double this number, finding a total of 25 O4–6.5 Ia supergiants within the Arches, with a further six objects of comparable spectral type assigned a luminosity class I–III to reflect a systematic reduction in emission line strength accompanied by an increase in strength of the Bry photospheric line.

3.2.3. O giants and main sequence stars

As discussed in Sect. 3.1 (and illustrated in Fig. 8), given the difficulty in distinguishing between main sequence and giant O stars we consider the remaining objects together. As with more luminous objects we employ the presence or otherwise of He I 2.112 μm and He II 2.189 μm absorption in conjunction with C IV 2.069 + 2.079 μm emission (where present) to constrain spectral type, while luminosity class diagnostics are outlined in Sect. 3.1. Direct comparison of observations to template spectra identifies six potential O giants (Figs. 4 and A.1) with spectral types ranging from \sim O5–6 (F96) to \sim O6–6.5 (F77). This conclusion is bolstered by comparison of the spectrum of F68 (O5.5–6 III) to the supergiant F29 (O5.5–6 Ia; Fig. 4); emission lines are systematically weaker while the Bry photospheric profile is deeper, with much more pronounced wings. We assign an intermediate (III–V) luminosity class to a further five stars (spanning the same range of

spectral types) where the comparatively low S/N compromises an assessment of the strength of the intrinsically weak C IV 2.079 μm line relative to the 2.11 μm emission blend. We also identify a population of stars which we tentatively classify as main sequence stars on the basis of the width and depth of the Bry line and, for the earliest spectral types, the absence of C IV emission even when other indicators of high temperature – such as strong He II 2.189 μm absorption and a lack of a He I 2.112 μm absorption component in the \sim 2.11 μm emission blend – are present (cf. Fig. 8). Examples are presented in Figs. 5 and 6, with the earliest examples being O5–6 V (e.g. F87). However, the relatively low S/N of many of these spectra complicates identification of features such as He II 2.189 μm and so greater uncertainty is associated with these spectral classifications. Indeed in a number of spectra Bry is the only line which may be confidently identified and hence we adopt a generic \geq O8 V classification for such stars, with the expectation that a number of stars may be substantially later (e.g. early-B) than this.

For completeness we highlight anomalies in the Bry profiles of a number of stars (Fig. A.1). F81 (O6–7 III–V) and, subject to the low S/N of the spectrum, F139 appear to show a sharp central emission peak superimposed on a broad photospheric profile. Likewise, infilling leads to an essentially flat continuum for F90 and F92 (both O5–6 V) and F93 (O5–6 III–V). Further observations will be required to assess the veracity of these features.

3.2.4. The absence of H-free WRs, LBVs, and interacting binaries

Finally, we consider the lack of certain types of evolved objects within the Arches. Turning first to H-free WRs, and if we are

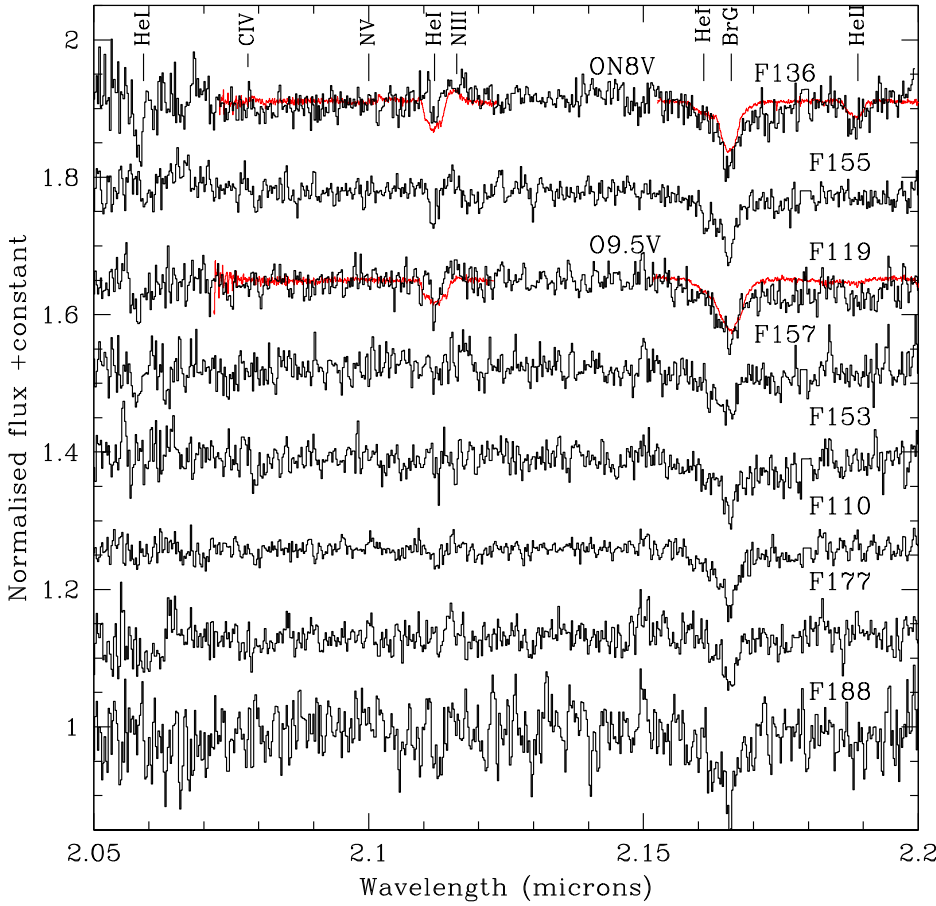


Fig. 6. Comparison of selected fainter cluster members (black) with MS K-band template spectra from Hanson et al. (2005; red).

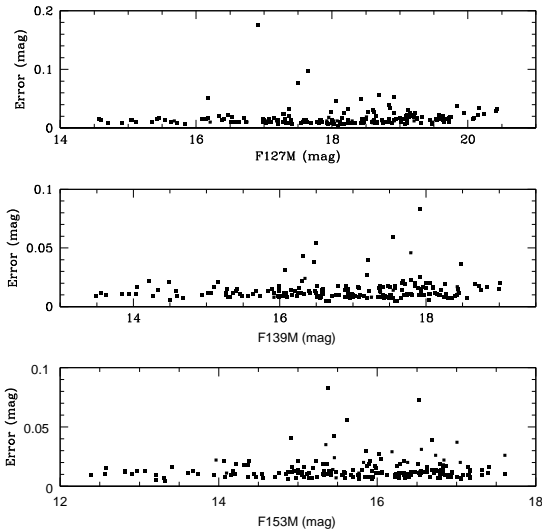


Fig. 7. Errors associated with the HST/WFC3 F127M, F139M and F153M photometry presented in Table A.1.

correct in our detection of the main sequence within the Arches, then we are reaching stars with $M_K \sim -4.4$ (O5 V) to ~ -3.3 (O9 V; Martins & Plez 2006). Consequently, the empirical values of M_K presented for both WN and WC field stars in Crowther et al. (2006) imply that, with the exception of the weak lined WN3-4 stars, we would expect to detect any H-free WN or WC stars within the Arches. Similar conclusions may be obtained upon consideration of the absolute near-IR magnitudes of the WR cohort within Wd1 (Crowther et al. 2006).

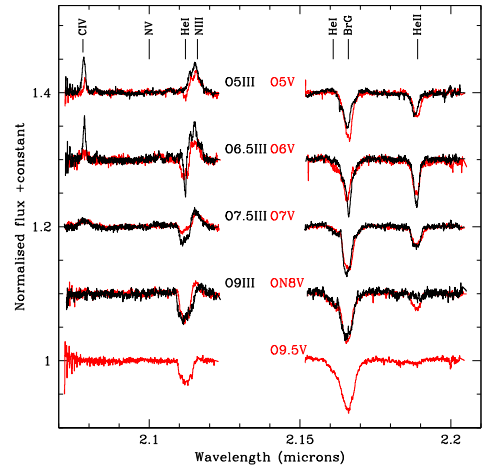


Fig. 8. Comparison of K-band classification spectra from Hanson et al. (2005) for mid-late O giant (black) and main sequence (red) stars. For earlier spectral types the strength of CIV relative to e.g. the $2.11 \mu\text{m}$ emission blend serves to distinguish between giants and main sequence stars, being weaker in the latter. For later spectral types one must rely on the shape of the Br γ profile, although this can be compromised by stellar rotational velocity.

Theoretical simulations support such an expectation. Groh et al. (2013) present M_K s for the pre-SN (WC or WO) end-points of single massive ($60\text{--}120 M_\odot$) stars which are in the range ($M_K \sim -3.3$ to -4.5) that we sample. Secondly Groh et al. (2014) present a detailed appraisal to the lifecycle of a single $60 M_\odot$ star and show that after spending ~ 3.2 Myr as an O supergiant it evolves through a variety of high luminosity phases

(blue hypergiant and luminous blue variable) before reaching H-free WN, WC, and finally WO states – all of which would be readily detectable in the Arches and are significantly longer-lived than the WNLh phase.

However, even if we are mistaken in our identification of the cluster main sequence, comparison of the Arches to the Quintuplet cluster is strongly suggestive of a lack of H-free WC stars. Located at a comparable distance and presumably observed through a similar extinction column, the Quintuplet has a rich population of WC stars (e.g. [Liermann et al. 2009](#)). Of these, the faintest, potentially single stars have $m_{F205W} \sim 11.3\text{--}11.7$ mag, while those found in binaries are significantly brighter still, ranging up to $m_{F205W} \sim 7.2$ mag (due to the formation of hot dust in the wind collision zone; [Clark et al. 2018](#)). In comparison we have spectral classifications for all stars to a limit of $m_{F205W} \sim 12.41$ mag (F31, Table A.1), strongly suggesting that no WC stars are present within the Arches at this time unless subject to particularly extreme differential reddening. Moreover, we may not easily appeal to the presence of such a star in a binary in which emission from the companion overwhelms it unless it is in such an orbital configuration that dust does not form and it is intrinsically fainter than examples within the Quintuplet. Trivially, similar conclusions may also be drawn from consideration of the massive field star population of the Galactic centre ([Mauerhan et al. 2010a](#); [Mauerhan et al. 2010b](#)) and the Galactic centre cluster ([Martins et al. 2007](#)).

Given the intrinsic IR luminosity of (candidate) luminous blue variables (LBVs) and cool hypergiants we can be sure that none are present within the Arches. Regarding LBVs; while it might be supposed that the Arches is too young for this phase to be encountered, the (pathological) LBV η Carina is located within the Trumpler 16/Collinder 228 stellar aggregate, which [Smith \(2006\)](#) show to contain a comparable stellar population of H-rich WNL and O stars to the Arches.

Lastly, while X-ray observations and our RV studies suggest that a number of (colliding wind) binaries are found within the cluster ([Wang et al. 2006](#), Papers II and III), the Arches appears to lack any systems in which rapid case-A mass-transfer is ongoing. Several examples of such systems have been proposed – Wd1-9 ([Clark et al. 2013b](#); [Fenech et al. 2017](#)), RY Scuti ([Gehrz et al. 1995, 2001](#); [Grundstrom et al. 2007](#)), NaSt1 ([Mauerhan et al. 2015](#)), and LHA 115-S 18 ([Clark et al. 2013a](#)) – and appear to manifest as (supergiant) B[e] stars (cf. discussion in [Kastner et al. 2010](#)), supporting a combination of a rich low excitation emission line spectrum and bright X-ray, IR, and sub-mm/radio continuum emission (due to colliding winds, the presence of hot dust and a highly elevated mass-loss rate, respectively). Such a combination of observational features would render such stars readily identifiable within the Arches, but none appear present.

4. The impact of an uncertain extinction law towards the Galactic centre

During the classification of cluster members we have intentionally excluded consideration of magnitudes due to the uncertainty in the correct interstellar reddening law to apply. Indeed we wish to utilise the main sequence cohort to better constrain reddening and so utilising photometric data in their identification would introduce a circularity into the argument.

Three issues beset attribution of interstellar reddening to individual stars: adoption of the correct reddening law, the presence of inhomogenous reddening across the cluster and an intrinsic IR-excess due to continuum emission from stellar winds. A number of studies have attempted to determine the

reddening law to the Galactic centre, with [Rieke & Lebofsky \(1985\)](#) providing the first optical-IR constraints. Their results were then generalised to a power-law formulation ($A_\lambda \propto \lambda^{-\alpha}$ with $\alpha = 1.61$) by [Cardelli et al. \(1989\)](#), although later studies utilising near-IR surveys ([Nishiyama et al. 2009](#)) and red-clump stars ([Schoedel et al. 2010](#)) suggest a steeper index of $\alpha = 2$. An alternative, derived for the nearby Quintuplet cluster from analysis of mid-IR data and based on the work of [Lutz \(1999\)](#), was described by [Moneti et al. \(2001\)](#); given the proximity of both clusters such a prescription could be appropriate for the Arches too.

[Habibi et al. \(2013\)](#) studied the reddening towards the Arches based upon the power-law formulation of [Rieke & Lebofsky \(1985; \$\alpha = 1.61\$ \)](#) and [Nishiyama et al. \(2009; \$\alpha = 2\$ \)](#) and demonstrated that extinction across the cluster is highly variable with no strong systematic trends as a function of location, ranging from $2.7 < A_K < 4.5$ mag and $2 < A_K < 3.4$ mag respectively. This has the potential to lead to large uncertainties in luminosity even before uncertainties in the intrinsic colour of individual stars due to wind emission are considered.

To emphasise the difficulty in constraining interstellar reddening and hence stellar luminosities, in Figs. 9 and A.2 we present the results of preliminary analysis of four of the WNLh stars, which are known to support strong stellar winds. We employ the CMFGEN non-LTE model atmosphere code of [Hillier & Miller \(1998, 1999\)](#) following the methodology described in [Najarro et al. \(2004\)](#). Spectroscopic data from the current paper were utilised as well as photometry from Table 1, Fi02 and [Dong et al. \(2011\)](#), paying particular attention to the bandpasses of individual filters. We adopted two prescriptions for the reddening law – a power-law for which the index was allowed to vary and that of [Moneti et al. \(2001\)](#).

The differences between best-fit models employing the two reddening laws are stark; in each case the power-law prescription results in a luminosity a factor of 3.4 (F7) to 4.5 (F6) times smaller than that derived under the assumption of the [Moneti et al. \(2001\)](#) law. While the luminosities derived from the latter are more in line with those derived from Ma08, given this gulf we refrain from discussing detailed model results for the physical properties of individual stars. However, more generally, we note that in each case the indices for the power-law prescription differ from one another, which is not expected on a physical basis, and are systematically steeper than previous derivations, leading to unexpectedly low stellar luminosities. We take both observations as a hint that this formulation does not provide a true description of either the reddening law or the stars themselves. However firm conclusions must await individually tailored quantitative analyses of a larger, statistically robust sample of cluster members.

Moreover, such an analysis also emphasises the role of differential reddening across the Arches. For the examples in this work the effect is limited, with extinction adopting the [Moneti \(power-law\)](#) prescription ranging from $A_K \sim 3.43\text{--}3.62$ for the WNLh stars considered, but [Lohr et al. \(2018\)](#) report $A_K \sim 4.52$ via an identical methodology for the similar object F2 – a range of ~ 1.2 mag. which reflects the results of [Habibi et al. \(2013\)](#).

5. Stellar and cluster properties

Given the significant uncertainties ($\Delta L_{\text{bol}} \sim 0.6$ dex) introduced by the lack of an accepted extinction law for the galactic centre, the effect of differential reddening ($\Delta L_{\text{bol}} \sim 0.4$ dex) as well as the effects of unrecognised binarity ($\Delta L_{\text{bol}} \sim 0.3$ dex) we refrain from constructing a cluster HR diagram at this time. As a consequence we are also unable to provide a quantitative

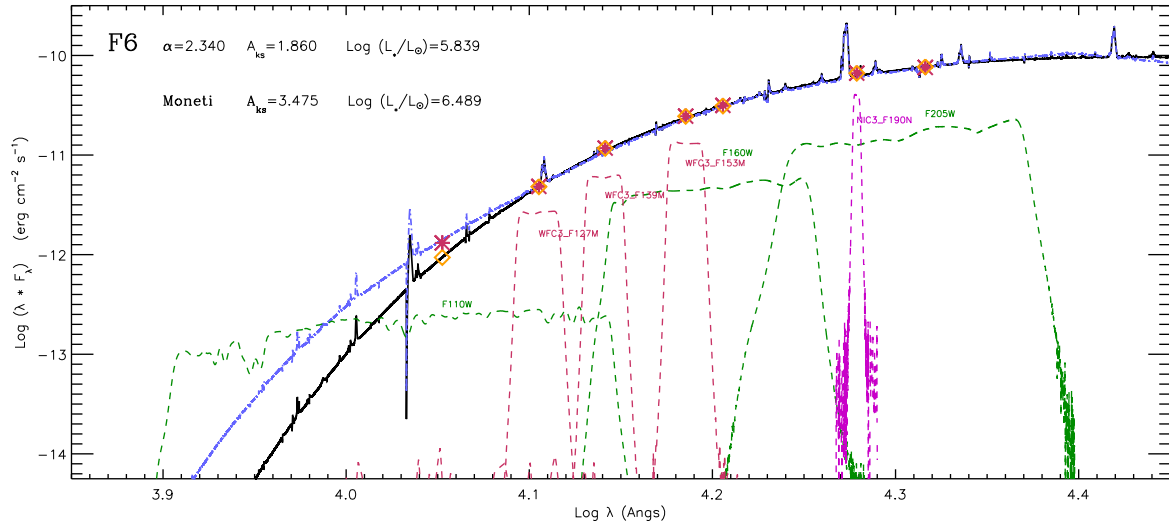


Fig. 9. Synthetic model-atmosphere spectra for the WNLh star F6 computed for two differing assumed interstellar reddening laws, illustrating the dramatic dependence of bolometric luminosity on this choice. HST photometry employed are from Table 1, Fi02 and Dong et al. (2011). The black line reflects the model spectrum that was reddened with $\alpha = 2.34$ which results in $A_{ks} = 1.860$, while the blue line follows Moneti’s law with $A_{ks} = 3.475$. Transmission curves for the filters used for the fit are shown in green (broad band) and pink (narrow band), and symbols are plotted for each magnitude measurement to show the goodness of fit: orange diamonds for the α -model and pink stars for the Moneti model. The x -axis position of each symbol corresponds to the classical λ_0 of the filter at which the zero-point flux is defined. The y -axis position coincides with its corresponding model curve if the observed magnitude matches the magnitude of the reddened model. Although the models differ considerably for $\text{Log } \lambda < 4.1$ (e.g. the F110W filter), they yield the same observed magnitudes. The reason for this is that, due to the high extinction, the reddened-SEDs fall off very steeply as λ decreases and as a result the effective wavelength of the filter moves to the red.

age estimate for the Arches from isochrone fitting, an estimate of masses for individual objects via comparison of current physical properties to evolutionary tracks and an accurately calibrated cluster luminosity function, or products derived from it, such as the (I)MF. In particular the errors in luminosity ($\Delta L_{\text{bol}} \sim 0.2$ dex) adopted by both Ma08 and Schneider et al. (2014) in their construction of an HR diagram and determination of the cluster (I)MF (respectively) appear to underestimated; leading to greater uncertainty in physical properties derived from these products.

The lack of such parameters are a serious impediment to exploiting the potential the Arches offers to probe the lifecycle of very massive stars; is there a high-mass truncation to its mass function and if so is it imposed by the physics of star formation/evolution or instead due to the most massive stars already having been lost to supernovae (SNe)? Given the magnitude of the uncertainties associated with current luminosity determinations, it is not immediately obvious how robust any extant age estimate for the Arches is (cf. Sect. 1). Such a situation is regrettable, since the ages determined by such studies currently straddle the threshold at which very massive stars may be expected to undergo SNe.

Despite these observational limitations, we may still utilise a combination of (i) dynamical mass estimates via cluster binaries and (ii) observational and/or theoretical calibration of the mapping between stellar mass and spectral type/luminosity class to estimate stellar masses. Similarly, age constraints may be imposed by comparison of the stellar content of the Arches to (i) those of other clusters for which age determinations via isochrone fitting have proved possible and (ii) the results of theoretical studies undertaken to determine the time at which stars of a given mass evolve through particular evolutionary phases. Before discussing this methodology in detail we highlight that the theoretical studies employ predictions based on the evolutionary pathways of single stars, which might be significantly

modified if instead a binary channel dominates (cf. Schneider et al. 2014).

5.1. Masses of cluster members

5.1.1. Dynamical masses

While a number of binary candidates have been identified within the Arches (Paper III), due to the limited temporal coverage of our dataset dynamical mass estimates have only been obtained for the components of the eclipsing SB2 system F2 (Paper II). This comprises a WN8-9h primary and O5-6 Ia⁺ secondary, with current masses of $\sim 82 \pm 12 M_{\odot}$ and $\sim 60 \pm 8 M_{\odot}$ respectively. Such an extreme mass for the primary is consistent with dynamical estimates for other hydrogen-rich WNLh stars¹¹, albeit subject to the twin caveats that these examples are of earlier spectral subtypes (possibly a function of differing metallicities) and that some lower mass examples are also known¹².

There are a similar handful of extreme O super-/hypergiants with dynamical mass determinations¹³. While caution has to be applied when considering HD 153919 – which is a product of binary evolution (Clark et al. 2002) – and the lower metallicity system R139, the mass of the secondary in F2 is also

¹¹ For example, the Galactic stars WR20a (WN6ha + WN6ha, $83 \pm 5 + 82 \pm 5 M_{\odot}$; Bonanos et al. 2004), WR21a (O3/WN5ha + O3 Vz((f*)), $> 64.4 \pm 4.8 + > 36.3 \pm 1.7 M_{\odot}$; Tramped et al. 2016) and NGC 3603-A1 (WN6ha + WN6ha, $116 \pm 31 + 89 \pm 16 M_{\odot}$; Schnurr et al. 2008).

¹² For example, WR22 (WN7ha + O8-9.5 III-V, $55.3 \pm 7.3 + 20.6 \pm 1.7 M_{\odot}$; Schweikhardt et al. 1999).

¹³ The Galactic systems LS III+46 11 (O3.5 If* + O3 If*, $> 38.8 \pm 0.8 + > 35.6 \pm 0.8 M_{\odot}$; Maíz-Apellániz et al. 2015), Cyg OB2 B17 (O7 Iaf⁺ + O9 Iaf, $60 \pm 5 + 45 \pm 4 M_{\odot}$; Stroud et al. 2010), the primary of the X-ray binary HD 153919 (O6.5Iaf*, $58 \pm 11 M_{\odot}$; Clark et al. 2002), and the LMC star R139 (O6.5Iafc + O6 Iaf, $> 78 \pm 8 + > 66 \pm 7 M_{\odot}$; Taylor et al. 2011).

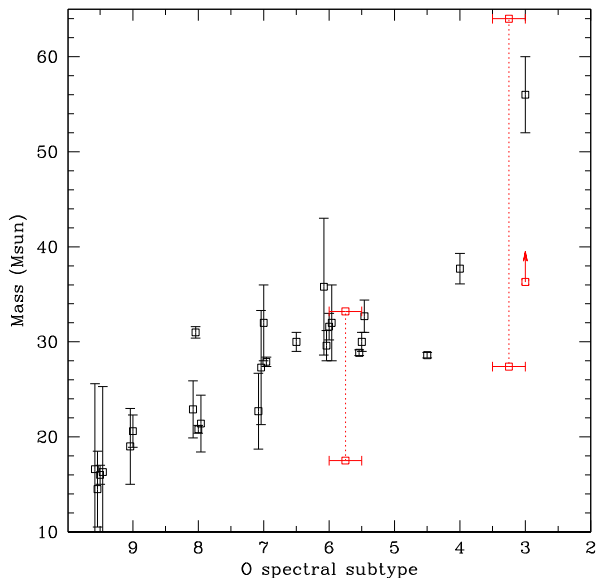


Fig. 10. Dynamical masses as a function of spectral type for main-sequence O stars. Symbols in black denote eclipsing systems as described in Sect. 5.1.1. Symbols in red denote the lower dynamical limit for the non-eclipsing secondary in WR21a and the primary and secondary components of HD 150136, with the dotted lines connecting to spectroscopic mass estimates for the latter two stars. Error bars for these two objects reflect uncertainties in their spectral type. Small offsets have been applied to individual stars of spectral types O5.5, O6, O7, O8, O9, and O9.5 for clarity.

fully consistent with these values; as with the WNLh stars, the early-mid O hypergiants also seem to have evolved from very massive progenitors.

Unfortunately we are only able to find dynamical mass estimates for a handful of O giants and supergiants, all of which are of later spectral type than found within the Arches¹⁴. Fortunately, significantly more dynamical estimates are available for main sequence O stars, and in Fig. 10 we present values from Weidner & Vink (2010); henceforth WeVi10) for galactic stars, supplemented by more recent determinations¹⁵. This indicates a broad linear relationship between mass and spectral type, with masses ranging from $\sim 20 M_{\odot}$ for O9 V stars through to $\sim 30\text{--}38 M_{\odot}$ for the earliest O5-6 V candidates identified within the Arches.

5.1.2. Theoretical calibration of the spectral type vs. stellar mass relation

In an effort to circumvent the lack of dynamical mass determinations WeVi10 and Martins & Palacios (2017; henceforth MaPa17) both utilised stellar evolutionary codes to predict the physical appearance of single stars of a given mass at a particular stage of their lifecycle. The former authors compare the

¹⁴ The primary of V729 Cyg (O7Ianf, $\sim 31.9 \pm 3.2 M_{\odot}$; Linder et al. 2009), the secondary of Wd1-13 (O9.5-B1 Ia; $35.4 \pm 5 M_{\odot}$; Ritchie et al. 2010), V1007 Sco A+B (O7.5 III + O7 III, $29.5 \pm 0.4 + 30.1 \pm 0.4 M_{\odot}$; Mayer et al. 2008), and CC Cas (O8.5 III, $35.4 \pm 5 M_{\odot}$; Gies 2003).

¹⁵ V382 Cyg (O7 V + O8 V, $27.9 \pm 0.5 + 20.8 \pm 0.4 M_{\odot}$; Yasarsoy & Yakut 2013), MY Cam (O4 V + O6 V, $37.7 \pm 1.6 + 31.6 \pm 1.4 M_{\odot}$; Lorenzo et al. 2014) and HD 150136 (O3-3.5 V((F^*)) + O5.5-6 V + O6.5-7 V((f)), $> 27.7 \pm 0.4 + > 17.5 \pm 0.3 M_{\odot}$; Mahy et al. 2012). Comparison of HD150135 to evolutionary predictions implies $\sim 64 M_{\odot}$ and $40 M_{\odot}$ respectively; both values are indicated in Fig. 10.

outputs of Geneva group models (e.g. luminosity, temperature; Meynet & Maeder 2003) to the spectral type and luminosity class calibrations of Martins et al. (2005). MaPa17 adopt a different approach, utilising the output of the STAREVOL code (Decressin et al. 2009; Armaed et al. 2016) as input for the non-LTE model atmosphere code CMFGEN (Hillier & Miller 1998, 1999). They use CMFGEN to generate a grid of synthetic spectra as a function of initial stellar mass and age, which then may be subject to spectral classification utilising the same criteria as employed for observational data.

MaPa17 provide evolutionary pathways for non-rotating stars of a given initial mass. They show that the main sequence population within the Arches arises from stars spanning $\sim 15 M_{\odot}$ (O9 V) to $\sim 30\text{--}40 M_{\odot}$ (O5-6 V). Stars with intermediate luminosity classes (II-IV) have initial masses ranging from $\sim 40\text{--}50 M_{\odot}$ (O6.5-7) to $\sim 50\text{--}60 M_{\odot}$ (O5-6). Finally the O4-5 Ia stars appear to evolve from very massive $\geq 80 M_{\odot}$ progenitors, while the handful of later O5-6.5 Ia stars are potentially consistent with an extension of this range to $\sim 60 M_{\odot}$ and above.

In contrast WeVi10 provide initial and current masses for both non-rotating and rotating stars of a given spectral type and luminosity class. The results for O9V stars – $\sim 14\text{--}24 M_{\odot}$ – are broadly compatible with the findings of MaPa17. However WeVi10 report a much wider mass range for O5-6 V stars; $\sim 26\text{--}53 M_{\odot}$ ($28\text{--}53 M_{\odot}$) for non-rotating (rotating) models. This trend continues through to supergiants, with WeVi10 suggesting that O4-5 Ia stars may derive from progenitors with masses of $58\text{--}120 M_{\odot}$ ($52\text{--}97 M_{\odot}$) for non-rotating (rotating) models, with current masses spanning $\sim 52\text{--}103 M_{\odot}$ ($43\text{--}74 M_{\odot}$) respectively. Such ranges differ significantly from the results of MaPa17 and, if confirmed, would appear to preclude the assignment of unique stellar masses based on spectral classification alone, especially for the earliest spectral types.

5.1.3. Summary - stellar masses for Arches members

Given the notable differences between the two theoretical studies summarised above, we assign primacy to dynamical mass estimates (Sect. 5.1.1). In doing so we suggest that both initial and current masses range from $\sim 15\text{--}20 M_{\odot}$ for the O8-9 V stars within the Arches, through to $\sim 30\text{--}40 M_{\odot}$ for the O5-6 V stars. These estimates are broadly consistent with the results of MaPa17. The current masses of the WN8-9h primary and O5-6 Ia⁺ secondary of F2 are consistent with other dynamical estimates for stars of comparable spectral type suggesting that the respective cluster cohorts are likewise of very high mass ($\sim 80 M_{\odot}$ and $\sim 60 M_{\odot}$ respectively), noting that neither theoretical study encompasses such stars. Finally the lack of dynamical estimates and the wide mass ranges suggested by WeVi10 and, to a lesser extent, by MaPa17, preclude the emplacement of robust values for the current masses of the Arches giant and supergiant populations, but one might reasonably expect them to lie between the preceding extremes (i.e. $\sim 40\text{--}60 M_{\odot}$).

It has long been established that the stellar winds of very massive stars significantly reduce their masses as they evolve away from the zero-age main sequence. This is evident in the Arches, where comparison to evolutionary calculations suggests that the WN8-9h primary of F2 was likely born with a mass of $\geq 120 M_{\odot}$ (Lohr et al. 2018, Paper II). Given that correction for this effect required an accurate determination of the current stellar parameters of F2, we refrain from inferring initial masses for the more evolved stellar cohorts (the remaining WNLh and O stars of luminosity classes I-III) within the Arches at this time.

5.2. Cluster age

5.2.1. Comparison to other clusters

While determining a cluster age via isochrone fitting is impossible at this juncture, we may utilise the presence – and absence – of stars of particular spectral types/luminosity classes to provide a qualitative estimate. The simplest approach is to compare the stellar content of the Arches to clusters with more accurate age estimates due to lower interstellar extinction (cf. the compilation by Clark et al. 2013b). Trivially, the lack of cool super/hypergiants suggests an age of <5 Myr (Clark et al. 2005). Fortunately, despite suffering from a similarly uncertain extinction, a more stringent constraint is provided by the Quintuplet cluster, which hosts a substantial $\sim O7$ -B0 supergiant population – while lacking the O4-6 supergiants found in the Arches – as well as a wealth of early B hypergiants and LBVs (Figer et al. 1999b; Liermann et al. 2009; Clark et al. 2018). These populations are absent from the Arches, suggesting that it is a younger system. Comparison to the studies of Groh et al. (2014) and MaPa17 suggests an age of ~ 3 – 3.6 Myr for the Quintuplet, which consequently would form an upper limit to the age of the Arches.

A lower bound to the age of the Arches is suggested by the apparent lack of stars with spectral type O2-3 of any luminosity class. Specifically, NGC 3603¹⁶, the apparently single aggregate comprising Trumpler 16 and Collinder 228¹⁷, Trumpler 14¹⁸ and R136 at the heart of the LMC star-forming region 30 Doradus¹⁹ all appear demonstrably younger than the Arches.

Nevertheless we are able to identify comparators, specifically Danks 1 ($1.5^{+1.5}_{-0.5}$ Myr; Davies et al. 2012) and potentially the lower mass aggregate Havlen Moffat 1 (~ 1.7 – 4 Myr; Massey et al. 2001; Vázquez & Baume 2001). Consequently such an approach yields a qualitative age determination broadly consistent with previous quantitative estimates, although critically not of sufficient precision to determine whether one would expect SNe to have already occurred.

5.2.2. Comparison to theoretical predictions

A related approach is to use the presence – or absence – of particular combinations of spectral types and luminosity classes in conjunction with theoretical predictions to infer ages for such stars. Trivially, such a methodology is susceptible to the same uncertainties in the evolutionary physics that afflicted the (analogous) determination of stellar masses in Sect. 5.1.2. Moreover the ingress and egress of cluster stars from a particular evolutionary phase is expected to be dependent on the distribution of stellar rotational velocities, which is unconstrained for the Arches.

Mindful of these caveats, and subject to uncertainties in the spectral classification, an obvious starting point is to utilise the location of the main sequence turn-off; given the possibility that very massive objects, such as the WNLha stars, may still be H-burning, we use this term with reference to a departure

¹⁶ Hosting six O3V, six O3 III, one O3.5Ifa, one O3If*/WN6 and three WN6ha stars for an assumed age of ~ 1 – 2 Myr (Drissen et al. 1995; Melena et al. 2008).

¹⁷ Hosting two O3.5 V((f)) stars and three WN6-7ha stars for an assumed age of ~ 2 – 3 Myr (Smith 2006).

¹⁸ Hosting one O2If* and three O3 V stars for an assumed age of ~ 1 – 2 Myr (Smith 2006).

¹⁹ Hosting three WN5h, one O2 If*/WN5, two O2 If, two O2 III-If, two O2-3III and 8 O2-3 V stars for an age of $1.5^{+0.3}_{-0.7}$ Myr (Crowther et al. 2016).

from luminosity class V. WeVi10 demonstrate that the apparent absence of main sequence stars of spectral class O4 and earlier implies a minimum age of ~ 2 Myr for the Arches for both rotating and non-rotating models. Conversely, WeVi10 suggest that O5 V (O6 V) stars evolve away from the MS after 2.4 (3.3) Myr; given their presence within the Arches this provides an upper limit to the cluster age.

Are the properties of the O supergiant and giant cohorts consistent with a cluster age in the range of 2–3.3 Myr? Turning first to the supergiants, and such a lower limit would be consistent with the absence of O3 I–III stars, which WeVi10 suggest disappear after 1.7 Myr. They further suggest that while non-rotating O4 supergiants vanish after ~ 2 Myr, rotating examples persist until 2.8 Myr, while non-rotating (rotating) O5 Ia stars may be expected until 2.5 Myr (3.4 Myr); both consonant with the age range inferred from the main sequence turn-off. Non rotating supergiants of spectral type O6 (6.5) first appear after 2.1 (2.2) Myr and so are also expected within this window. Thus, depending on the distribution of rotational velocities and given the uncertainties in spectral classification, the properties of the supergiant cohort are indeed consistent with an age of ~ 2.0 – 3.3 Myr.

Interpreting the prospective giant population is more difficult given current observational uncertainties. Broadly speaking, the time of the first appearance of giants with spectral classifications earlier than $\sim O6$ is consistent with the upper limit(s) to the cluster age; however objects with spectral types later than $\sim O6.5$ – 7 might be expected to appear at later times. Consequently if stars such as F85 (O7-8 III–V) are found to be giants they may be in tension with the constraints implied by the main sequence population.

Unfortunately, no theoretical predictions for the ages of the hypergiant and WNL populations are available to test their compatibility with these estimates.

We may, however, utilise the apparent lack of WC (or other hydrogen-free) stars, LBVs and B-type hypergiants within the Arches to provide additional constraints (Sect. 3.2.4). The absence of WC stars implies that cluster members have yet to reach this evolutionary stage and, since it is thought to almost immediately precede core-collapse, it appears likely that SNe also have yet to occur. Groh et al. (2013) provide simulations of massive stars that yield the time at which SNe take place as a function of initial stellar mass. For $120 M_{\odot}$ stars – implied by the primary of F2 (Sect. 5.1.1) – these suggest that SNe first occur between 3 and 3.55 Myr (for non-rotating and rotating models); if the above assertions are correct the latter serves as an upper limit to the cluster age²⁰.

In a related study Groh et al. (2014) provide the full evolutionary sequence for a non-rotating $60 M_{\odot}$ star, showing that a combined B-type hypergiant/LBV phase is encountered between ~ 3.25 and 3.56 Myr ($\sim 10\%$ of the lifetime of the preceding O supergiant phase). Since we may confidently expect stars of $60 M_{\odot}$ to have formed within the Arches (Sect. 5.1) we can assume that they have yet to evolve this far and consequently that the cluster is likely to be younger than ~ 3.2 Myr.

To summarise – we infer a current age for the Arches of ~ 2 – 3.3 Myr from the apparent position of the main sequence turn-off. As far as we may determine, such a value is consistent with (i) the age of $\sim 2.6^{+0.4}_{-0.2}$ Myr obtained for the eclipsing SB2

²⁰ Unfortunately Groh et al. (2013) do not provide timings for the onset of the WC phase for stars $\geq 85 M_{\odot}$ and so we cannot allow for its duration in our age determinations, although we note that for $\geq 60 M_{\odot}$ stars Groh et al. (2014) show the WC phase persists for ~ 0.2 Myr prior to SN.

binary F2 (Paper II), (ii) the properties of the more evolved stars within the Arches – such as the supergiant cohort, (iii) the lack of LBVs and H-free Wolf–Rayets such as the WC and WO subtypes and (iv) the ages determined for other young massive clusters with similar stellar populations. Within the uncertainties it is also consistent with previously published determinations, albeit lying at the lower end of the resultant span of age estimates.

Furthermore given the absence of an H-free stellar cohort we consider it unlikely that the cluster is at an age at which SNe are regularly occurring, although we cannot exclude the possibility that a handful of unusually massive ($\gg 120 M_{\odot}$) stars have already been lost to such events.

6. Discussion

As previously discussed the most noteworthy features of our spectroscopic dataset appear to be the continuous and smooth progression of spectral morphologies from intrinsically luminous to less luminous cluster members and the absence of any star more evolved than the WNLh cohort. To these we may add the apparent lack of massive blue stragglers within the cluster. Specifically no stars with spectral types O2-3, such as those seen in e.g. NGC 3603 and R136, are present (footnotes 16 and 19 and Crowther & Walborn 2011). Likewise no WN5-6h stars are found within the Arches, although they have been identified in younger clusters such as NGC 3603 (Melena et al. 2008).

What constraints do such observations place on stellar evolution? The distribution of spectral types amongst the candidate main sequence and giant stars is consistent with single star evolution and the simulations of Schneider et al. (2014) which imply that the majority of stars in the $\sim 32\text{--}50 M_{\odot}$ window are pre-interaction systems. However the situation differs for supergiants and more luminous/evolved stars. Ma08 interpret the distribution of spectral types under the paradigm of single star evolution, suggesting that they are consistent with an evolutionary sequence progressing from O supergiant through O hypergiant to WNha star (for masses $>60 M_{\odot}$), with the latter stars evolving from earlier (O2-3) supergiants than are currently present within the Arches. Conversely, Schneider et al. (2014) suggest – under the assumption of a 100% initial binary fraction – that the WNha stars are instead binary products.

Two observational findings cast light on these assertions. Firstly there is a smooth progression from O supergiants with infilled Bry absorption (e.g. F20, F33, and B4; Fig. 3) through the least extreme hypergiants (e.g. F18, F27, and F40; Fig. 2) to those with the strongest emission in Bry (F10, F17 and the secondary in F2; Fig. 2) which in turn are almost indistinguishable from WNLha stars such as F16 (Fig. 1). The development of increased emission in Bry is indicative of a progressively denser stellar wind across these spectral types and reinforces the supposition that the hypergiants indeed bridge the gap between the O supergiant and WNLha stars. Secondly the physical properties of the eclipsing binary F2 suggest it is in a pre-interaction phase (Paper II). Analysis of its lightcurve suggests that it is just entering a contact phase with the orbit found to be slightly eccentric. Moreover the current WN8-9h primary of F2 appears in a more evolved phase than the O4-5Ia⁺ secondary; if it were the product of mass transfer the reverse would be the case.

As a consequence we strongly suspect that at least some of the WNLh cohort are indeed the product of the single star evolutionary channel proposed by Ma08. However, the presence of F2 and the hard X-ray emission from a number of other WNh stars is clearly indicative of a binary population amongst these objects (Wang et al. 2006). Consequently one might ask where the

post-interaction binaries are given that Schneider et al. (2014) suggest that on average the most massive star in an Arches-like cluster would be expected to be a binary product after only ~ 1 Myr?

Obvious routes to lower the expected number of blue stragglers would be to reduce one or more of the cluster mass, age or binary fraction and/or to steepen the initial mass function. However if exceptionally massive stars always present as WN7-9h in high metallicity environments such as the Galactic centre, rather than the WN5-6h objects seen in e.g. NGC 3603 and R136, one could suppose that blue stragglers are hidden in plain sight amongst the most luminous examples of this population.

7. Conclusions

In this paper we present the first results of a multi-epoch spectroscopic survey of the Arches cluster, co-adding multiple spectra to obtain the deepest observations ever of the stellar population. We supplement these with new HST photometric data for confirmed and candidate cluster members. Excluding interlopers and those objects with low S/N and/or blended spectra, we provide spectral classifications for 88 cluster members, an increase in sample size over Ma08 by a factor of ~ 3 . We find no further WRs of any subtype in the cluster; importantly, no H-free stars have been identified. In contrast we expand the number of cluster O hypergiants from two to eight and supergiants from 11 to 25; the largest population of any known Galactic cluster. The greater S/N of these data allow us to refine previous classifications but, as with Ma08, no examples of supergiants with spectral type earlier than O4 or later than O6.5 are found. Extending the sequence of morphologically similar spectra to fainter objects, we are able to identify a population of intermediate (I–III) luminosity class stars which smoothly segues into a cohort of giants with spectral types covering the same range as the supergiants. Finally we identify a number of fainter objects which we classify as main sequence stars, with spectral types ranging from O5-6 V to \geq O8 V. This implies a main-sequence turn-off between O4-5 V (where we employ this term to refer specifically to luminosity class V objects, since it is suspected that some evolved, very massive stars may still be core H-burning; e.g. Smith & Conti 2008).

Provisional analysis of a number of the WNLh stars reveals that a combination of uncertainty in the correct extinction law to apply and differential reddening across the cluster leads to unexpectedly large errors in luminosity ($\Delta L_{\text{bol}} \sim 0.6$ dex and ~ 0.4 dex, respectively). While our results favour a Moneti rather than a power-law formulation for the extinction law, accurate determination of the stellar parameters of cluster members requires modelling of individual objects, beyond the scope of this work. As such we are not able to make direct comparison to theoretical isochrones to determine a cluster age, calibrate the (I)MF or determine an integrated cluster mass, and urge caution with regard to previous determinations – and conclusions resulting from them – given that uncertainties employed in their calculation have been systematically underestimated.

Nevertheless we are able to estimate stellar and cluster properties from the current data. Specifically the dynamical masses of the WN8-9h+O4-6Ia⁺ binary F2 (Paper II) suggest current masses of ~ 80 and $\sim 60 M_{\odot}$ for the WNLh and O hypergiant cohorts respectively. Comparison of the stellar properties of the WN8-9h primary to evolutionary tracks suggests an initial mass of $\geq 120 M_{\odot}$ (Paper II), providing strong support for the modification of the upper reaches of the current mass function due to mass-loss (cf. Schneider et al. 2014). Empirical calibration of the spectral type/mass relation for main sequence

stars suggests a main-sequence turn-off in excess of $\sim 30\text{--}38 M_{\odot}$. Consequently, excluding the 13 stars which we classify as $\geq O8 V$, the Arches appears to contain at least 75 stars with initial masses $\geq 30 M_{\odot}$, with the masses of the super-/hypergiants and WNLh stars greatly in excess of this value.

The main sequence turn-off suggests a cluster age of $\sim 2\text{--}3.3$ Myr, broadly consistent with the properties of the more evolved population of the cluster, including the eclipsing binary F2 (Paper II). Notably, the lack of H-free WRs, BHGs, and LBVs strongly argues against ages much larger than this. Comparison to the Quintuplet also suggest an upper limit to the age of the Arches of ≤ 3.6 Myr (Clark et al. 2018), consistent with the above results. Unfortunately these estimates still bracket the ages at which one might expect the first SNe to occur for very massive stars ($\geq 120 M_{\odot}$). An expanded sample of high S/N spectra of main sequence stars would help refine this critical parameter.

The smooth evolution in spectral morphologies transiting from O supergiant through the greatly expanded hypergiant population to the WNLh stars, when combined with the properties of the apparently pre-interaction binary F2, argues for the prevalence of a single star evolutionary pathway within the cluster at this time. Nevertheless the presence of a number of very massive binaries (Sect. 6 and Paper III) suggests that a binary channel may well play an important (future) role. Despite predictions that binary products may be present within the cluster after only ~ 1 Myr we see no systems currently exhibiting mass-transfer nor blue stragglers, unless both single and binary evolution yield superficially identical WNLh stars.

In conclusion the combination of the relative proximity, age and the rich stellar population of the Arches makes it a unique laboratory for studying the evolution of very massive stars via both single and binary evolutionary channels as well as star formation in the extreme environment of the Galactic centre. In particular we may hope to constrain the upper mass limit for very massive stars, determine how they form (and/or how they subsequently grow via binary interaction) and elucidate the physical properties of this population. All of these goals are essential for quantifying chemical, mechanical and radiative feedback in both the local and early Universe; moreover, such stars are the prime candidates for pair-instability SNe, GRBs and ultimately coalescing binary black holes. However in order to fulfil the potential of the Arches in these regards we must first constrain the properties of the binary population and the physical parameters of the constituent stars via individual quantitative modelling: goals that will be addressed in future papers in this series.

Acknowledgements. Based on observations collected at the European Organisation for Astronomical Research in the Southern Hemisphere under ESO programmes 087.D-0317, 091.D-0187, and 099.D-0345. This research was supported by the Science and Technology Facilities Council. FN acknowledges financial support through Spanish grants ESP2015-65597-C4-1-R and ESP2017-86582-C4-1-R (MINECO/FEDER). We thank Chris Evans and Paul Crowther for their valuable comments. Finally we thank the referee, Ben Davies, for his careful reading and insightful comments, which significantly improved the manuscript.

References

- Armaed, L., Palacios, A., Charbonnel, C., Gallet, F., & Bouvier, J. 2016, *A&A*, **587**, A105
- Blum, R. D., Schaerer, D., Pasquali, A., et al. 2001, *AJ*, **122**, 1875
- Bonanos, A. Z., Stanek, K. Z., Udalski, A., et al. 2004, *ApJ*, **611**, L33
- Bonnell, I. A., Bate, M. R., Clarke, C. J., & Pringle, J. E. 2001, *MNRAS*, **323**, 785
- Bonnet, H., Abuter, R., Baker, A., et al. 2004, *The Messenger*, **117**, 17
- Cardelli, J. A., Clayton, G. C., & Mathis, J. S. 1989, *ApJ*, **345**, 245
- Clark, J. S., Goodwin, S. P., Crowther, P. A., et al. 2002, *A&A*, **392**, 909
- Clark, J. S., Negueruela, I., Crowther, P. A., & Goodwin, S. P. 2005, *A&A*, **434**, 949
- Clark, J. S., Ritchie, B. W., Negueruela, I., et al. 2011, *A&A*, **531**, A28
- Clark, J. S., Bartlett, E. S., Coe, M. J., et al. 2013a, *A&A*, **560**, A10
- Clark, J. S., Ritchie, B. W., & Negueruela, I. 2013b, *A&A*, **560**, A11
- Clark, J. S., Ritchie, B. W., Najarro, F., Langer, N., & Negueruela, I. 2014, *A&A*, **567**, A73
- Clark, J. S., Lohr, M. E., Patrick, L. R., et al. 2018, *A&A*, in press, DOI: [10.1051/0004-6361/201833041](https://doi.org/10.1051/0004-6361/201833041)
- Clarkson, W. I., Ghez, A. M., Morris, M. R., et al. 2012, *ApJ*, **751**, 132
- Cotera, A. S., Erickson, E. F., Colgan, S. W. J., et al. 1996, *ApJ*, **461**, 750
- Crowther, P. A., & Furness, J. P. 2008, *A&A*, **492**, 111
- Crowther, P. A., & Walborn, N. R. 2011, *MNRAS*, **416**, 1311
- Crowther, P. A., Hadfield, L. J., Clark, J. S., Negueruela, I., & Vacca, W. D. 2006, *MNRAS*, **372**, 1407
- Crowther, P. A., Schnurr, O., Hirschi, R., et al. 2010, *MNRAS*, **408**, 731
- Crowther, P. A., Caballero-Nieves, S. M., Bostroem, K. A., et al. 2016, *MNRAS*, **458**, 624
- Davies, B., Clark, J. S., Trombly, C., et al. 2012, *MNRAS*, **419**, 1871
- Decressin, T., Mathis, S., Palacios, A., et al. 2009, *A&A*, **495**, 271
- de Mink, S. E., Sana, H., Langer, N., Izzard, R. G., & Schneider, F. R. N. 2014, *ApJ*, **782**, 7
- Dolphin, A. E. 2000, *PASP*, **112**, 1383
- Dong, H., Wang, Q. D., Cotera, A., et al. 2011, *MNRAS*, **417**, 114
- Dong, H., Schödel, R., Williams, B. F., et al. 2017, *MNRAS*, **470**, 3427
- Drissen, L., Moffat, A. F. J., Walborn, N. R., & Shara, M. M. 1995, *AJ*, **110**, 2235
- Eisenhauer, F., Abuter, R., Bickert, K., et al. 2003, in *Instrument Design and Performance for Optical/Infrared Ground-based Telescopes*, eds. M. Iye, & A. F. M. Moorwood, *SPIE Conf. Ser.*, **4841**, 1548
- Espinoza, P., Selman, F. J., & Melnick, J. 2009, *A&A*, **501**, 563
- Fenech, D. M., Clark, J. S., Prinja, R. K., et al. 2017, *MNRAS*, **464**, L75
- Figer, D. F., McLean, I. A., & Morris, M. 1999a, *ApJ*, **514**, 202
- Figer, D. F., Kim, S. S., Morris, M., et al. 1999b, *ApJ*, **525**, 750
- Figer, D. F., Najarro, F., Gilmore, D., et al. 2002, *ApJ*, **581**, 258 (Fi02)
- Gehrz, R. D., Hayward, T. L., Houck, J. R., et al. 1995, *ApJ*, **439**, 417
- Gehrz, R. D., Smith, N., Jones, B., Puetter, R., & Yahil, A. 2001, *ApJ*, **559**, 395
- Gies, D. R. 2003, in *A Massive Star Odyssey: From Main Sequence to Supernova*, eds. K. van der Hucht, A. Herrero, & C. Esteban, *IAU Symp.*, **212**, 91
- Groh, J. H., Meynet, G., Georgy, C., & Ekström, S. 2013, *A&A*, **558**, A131
- Groh, J. H., Meynet, G., Ekström, S., & Georgy, C. 2014, *A&A*, **564**, A30
- Grundstrom, E. D., Gies, D. R., Hellwig, T. C., et al. 2007, *ApJ*, **667**, 505
- Habibi, M., Stolte, A., Brandner, W., Hußman, B., & Motohara, K. 2013, *A&A*, **556**, A26
- Hanson, M. M., Conti, P. S., & Rieke, M. J. 1996, *ApJS*, **107**, 281
- Hanson, M. M., Kudritzki, R.-P., Kenworthy, M. A., Puls, J., & Tokunaga, A. T. 2005, *ApJS*, **161**, 154
- Hillier, D. J., & Miller, D. L. 1998, *ApJ*, **496**, 407
- Hillier, D. J., & Miller, D. L. 1999, *ApJ*, **519**, 354
- Horne, K. 1986, *PASP*, **98**, 609
- Kastner, J. H., Buchanan, C., Sahai, R., Forrest, W. J., & Sargent, B. A. 2010, *AJ*, **139**, 1993
- Kim, S. S., Figer, D. F., Kudritzki, R. P., & Najarro, F. 2006, *ApJ*, **653**, L113
- Lang, C. C., Johnson, K. E., Goss, W. M., & Rodríguez, L. F. 2005, *AJ*, **130**, 2185
- Liermann, A., Hamann, W.-R., & Oskinova, L. M. 2009, *A&A*, **494**, 1137
- Liermann, A., Hamann, W.-R., & Oskinova, L. M. 2014, *A&A*, **540**, A14
- Linder, N., Rauw, G., Manford, J., et al. 2009, *A&A*, **495**, 231
- Lohr, M. E., Clark, J. S., Najarro, F., et al. 2018, *A&A*, **617**, A66 (Paper II)
- Lorenzo, J., Negueruela, I., Baker, A. F. K. Val, et al. 2014, *A&A*, **572**, A110
- Lutz, D. 1999, *The Universe as Seen by ISO*, eds. P. Cox, & M. F. Kessler, *ESA SP*, **427**, 623
- Mahy, L., Gosset, E., Sana, H., et al. 2012, *A&A*, **540**, A97
- Maíz-Apellániz, J., Negueruela, I., Barbá, R. H., et al. 2015, *A&A*, **579**, A108
- Martins, F., & Palacios, A. 2017, *A&A*, **598**, A56
- Martins, F., & Plez, B. 2006, *A&A*, **457**, 637
- Martins, F., Schaerer, D., & Hillier, D. J. 2005, *A&A*, **436**, 1049
- Martins, F., Genzel, R., Hillier, D. J., et al. 2007, *A&A*, **468**, 233
- Martins, F., Hillier, D. J., Paumard, T., et al. 2008, *A&A*, **478**, 219
- Massey, P., DeGioia-Eastwood, K., & Waterhouse, E. 2001, *AJ*, **121**, 1050
- Mauerhan, J. C., Munro, M. P., Morris, M. R., Stolovy, S. R., & Cotera, A. 2010a, *ApJ*, **710**, 706
- Mauerhan, J. C., Cotera, A., Dong H., et al. 2010b, *ApJ*, **725**, 188
- Mauerhan, J. C., Smith, N., Van Dyk, S. D., et al. 2015, *MNRAS*, **450**, 2551
- Mayer, P., Harmanec, P., Nesslinger, S., et al. 2008, *A&A*, **481**, 183

- Melena, N. W., Massey, P., Morrell, N. I., & Zangari, A. M. 2008, *AJ*, **135**, 878
- Meynet, G., & Maeder, A. 2003, *A&A*, **404**, 975
- Moneti, A., Stolovy, S., Blommaert, J. A. D. L., Figer, D. F., & Najarro, F. 2001, *A&A*, **366**, 106
- Nagata, T., Woodward, C. E., Shure, M., & Kobayashi, N. 1995, *AJ*, **109**, 1676
- Najarro, F., Figer, D. F., Hillier, D. J., & Kudritzki, R. P. 2004, *ApJ*, **611**, L105
- Negueruela, I., Marco, A., Herrero, A., & Clark, J. S. 2008, *A&A*, **487**, 575
- Negueruela, I., Clark, J. S., & Ritchie, B. W. 2010, *A&A*, **516**, A78
- Nishiyama, S., Tamura, M., Hatano, H., et al. 2009, *ApJ*, **696**, 1407
- Rieke, G. H., & Lebofsky, M. J. 1985, *ApJ*, **288**, 618
- Ritchie, B. W., Clark, J. S., Negueruela, I., & Langer, N. 2010, *A&A*, **516**, A78
- Rosslowe, C. K., & Crowther, P. A. 2018, *MNRAS*, **473**, 2853
- Sana, H., de Mink, S. E., de Koter, A., et al. 2012, *Science*, **337**, 444
- Schneider, F. R. N., Izzard, R. G., de Mink, S. E., et al. 2014, *ApJ*, **780**, 117
- Schneider, F. R. N., Izzard, R. G., Langer, N., & de Mink, S. E. 2015, *ApJ*, **805**, 20
- Schnurr, O., Casoli, J., Chené, A.-N., Moffat, A. F. J., & St-Louis, N. 2008, *MNRAS*, **389**, L38
- Schoedel, R., Najarro, F., Muzic, K., & Eckart, A. 2010, *A&A*, **511**, A18
- Schweikhardt, J., Scmutz, W., Stahl, O., Szeifert, Th., & Wolf, B. 1999, *A&A*, **347**, 127
- Serabyn, E., Shupe, D., & Figer, D. F. 1998, *Nature*, **394**, 448
- Shu, F. H., Adams, F. C., & Lizano, S. 1987, *ARA&A*, **25**, 23
- Smith, N. 2006, *MNRAS*, **367**, 763
- Smith, N., & Conti, P. S. 2008, *ApJ*, **679**, 1467
- Stolte, A., Grebel, E. K., Brandner, W., & Figer, D. F. 2002, *A&A*, **394**, 459
- Stolte, A., Brandner, W., Grebel, E. K., Lenzen, R., & Lagrange, A.-M. 2005, *ApJ*, **628**, L113
- Stroud, V. E., Clark, J. S., Negueruela, I., et al. 2010, *A&A*, **511**, A84
- Taylor, W. D., Evans, C. J., Sana, H., et al. 2011, *A&A*, **530**, L10
- Tramper, F., Sana, H., Fitzsimons, N. E., et al. 2016, *MNRAS*, **455**, 1275
- van Bever, J., & Vanbeveren, D. 1998, *A&A*, **334**, 21
- Vázquez, R. A., & Baume, G. 2001, *A&A*, **371**, 908
- Wang, Q. D., Dong, H., & Lang, C. 2006, *MNRAS*, **371**, 38
- Weidner, C., & Vink, J. S. 2010, *A&A*, **524**, A98
- Wright, N. J., Drew, J. E., & Mohr-Smith, M. 2015, *MNRAS*, **449**, 741
- Yasarsoy, B., & Yakut, K. 2013, *AJ*, **145**, 9
- Zinnecker, H., & Yorke, H. W. 2007, *ARA&A*, **45**, 481

Appendix A: Additional material

Table A.1. The stellar population of the Arches cluster.

ID	RA (h m s)	Dec (d m s)	m_{F127M} (mag)	m_{F139M} (mag)	m_{F153M} (mag)	m_{F205W} (mag)	#Observations (#Epochs)	Spec. class.	Notes
B1	17 45 51.50	-28 49 26.8	–	–	–	–	5(5)	WN8-9h	
B4	17 45 50.86	-28 49 19.7	–	–	–	–	15(10)	O5.5-6 Ia	
F1	17 45 50.260	-28 49 22.76	15.45	14.21	12.97	10.45	10(9)	WN8-9h	Radio ¹
F2	17 45 49.746	-28 49 26.29	16.73	15.29	13.94	11.18	15(14)	WN8-9h	SB2, Radio, X-ray
								O5-6 Ia ⁺	
F3	17 45 50.884	-28 49 26.89	15.05	13.94	12.81	10.46	5(5)	WN8-9h	Radio
F4	17 45 50.628	-28 49 18.10	14.57	13.56	12.56	10.37	26(10)	WN7-8h	Radio
F5	17 45 50.510	-28 49 32.40	15.68	14.50	13.32	10.86	5(5)	WN8-9h	Radio ¹
F6	17 45 50.478	-28 49 22.79	14.60	13.49	12.39	10.37	13(5)	WN8-9h	Radio ¹ , X-ray
F7	17 45 50.529	-28 49 20.03	14.71	13.63	12.58	10.48	26(10)	WN8-9h	X-ray
F8	17 45 50.447	-28 49 21.75	15.12	14.03	12.91	10.76	8(5)	WN8-9h	Radio
F9	17 45 50.321	-28 49 12.26	14.91	13.85	12.82	10.77	10(10)	WN8-9h	X-ray
F10	17 45 50.121	-28 49 27.01	16.21	14.93	13.74	11.46	5(5)	O7-8 Ia ⁺	
F12	17 45 50.337	-28 49 17.78	15.35	14.26	13.21	10.99	13(10) ^b	WN7-8h	
F13	17 45 50.102	-28 49 24.15	16.52	15.28	14.08	11.74	5(5)	O7-8 Ia ⁺	
F14	17 45 50.735	-28 49 23.08	15.43	14.34	13.31	11.72	12(5)	WN8-9h	
F15	17 45 50.811	-28 49 17.09	15.07	14.05	13.07	11.27	20(11)	O6-7 Ia ⁺	
F16	17 45 50.581	-28 49 21.17	15.55	14.48	13.42	11.40	11(5)	WN8-9h	
F17	17 45 50.192	-28 49 27.66	17.03	15.73	14.47	12.15	5(5)	O5-6 Ia ⁺	
F18	17 45 50.532	-28 49 18.42	15.63	14.59	13.61	11.63	23(10)	O4-5 Ia ⁺	Radio
F19	17 45 49.818	-28 49 26.48	17.92	16.53	15.18	12.60	14(13)	O4-5 Ia	Radio
F20	17 45 50.481	-28 49 20.18	16.53	15.41	14.38	12.16	20(10)	O4-5 Ia	
F21	17 45 50.820	-28 49 20.11	15.72	14.67	13.68	11.77	22(10)	O6-6.5 Ia	
F22	17 45 50.278	-28 49 17.21	16.42	15.26	14.16	12.02	9(9) ^a	O5.5-6 Ia	
F23	17 45 51.211	-28 49 23.84	16.38	15.27	14.21	12.19	1(1)	O6-6.5 Ia	
F24	17 45 50.152	-28 49 21.21	17.29	16.06	14.88	12.61	6(6) ^c	O4-5 Ia	
F25	17 45 50.012	-28 49 27.06	18.35	16.93	15.57	13.05	9(9) ^b	O4-5 Ia	
F26	17 45 50.610	-28 49 24.03	16.61	15.46	14.37	12.34	8(5)	O4-5 Ia	
F27	17 45 50.664	-28 49 20.02	16.09	15.01	13.97	12.01	29(10)	O4-5 Ia ⁺	
F28	17 45 50.699	-28 49 22.21	16.17	15.07	14.06	12.17	13(5)	O4-5 Ia	
F29	17 45 50.799	-28 49 18.14	16.14	15.10	14.10	12.26	22(11)	O5.5-6 Ia	
F30	17 45 50.275	-28 49 19.10	16.75	15.63	14.56	12.53	10(8) ^c	O4-5 Ia	
F31	17 45 50.478	-28 49 20.16	–	–	–	12.41	–	–	
F32	17 45 50.681	-28 49 20.35	16.46	15.41	14.37	12.42	13(5)	O4-5 Ia	
F33	17 45 50.723	-28 49 20.40	16.38	15.32	14.32	12.42	13(5)	O4-5 Ia	
F34	17 45 50.863	-28 49 21.54	16.54	15.48	14.44	12.49	6(5) ^b	O4-5 Ia	
F35	17 45 50.755	-28 49 17.50	16.17	15.15	14.18	12.37	20(11)	O4-5 Ia	
F36	17 45 49.789	-28 49 07.89	18.03	16.58	15.13	12.60	–	–	
F37	17 45 50.529	-28 49 19.77	–	–	–	12.63	–	–	Radio ¹
F38	17 45 50.755	-28 49 20.48	16.33	15.36	14.22	12.38	11(5)	O4-5 Ia	
F39	17 45 51.166	-28 49 36.70	16.98	15.84	14.76	12.65	–	–	
F40	17 45 50.685	-28 49 18.83	16.63	15.57	14.55	12.67	27(11)	O4-5 Ia ⁺	
F41	17 45 50.429	-28 49 27.42	18.46	17.15	15.89	13.53	–	–	
F42	17 45 50.364	-28 49 21.24	16.99	15.89	14.85	12.82	10(8)	O4-5 Ia	
F43	17 45 50.546	-28 49 19.17	17.28	16.21	15.19	13.04	25(11)	O4-5 Ia	
F44	17 45 50.701	-28 49 25.59	17.19	16.05	14.93	12.88	5(3)	–	Blend
F45	17 45 50.497	-28 49 24.25	17.33	16.16	15.07	13.01	10(5)	O4-5 Ia	

Notes. Column 1 indicates the nomenclature for cluster members adopted by Fi02 and Blum et al. (2001), cols. 2 and 3 the J2000 coordinates, cols. 4–6 the new HST WFC3 photometry described in Sect. 2.2 and col. 7 F205W filter photometry from Fi02. Column 8 presents the total number of VLT/SINFONI data-cubes available for individual objects, with the number in parentheses being the number of epochs on which these data were obtained (^{a,b,c}) denotes that, respectively, 1, 2, or 3 epochs of spectroscopy were not employed due to low S/N). Column 9 provides a spectral classification where spectra are available, while the final column provides additional notes including the presence of radio (data from Lang et al. 2005, where ⁽¹⁾ denotes a radio variable source) and X-ray detections Wang et al. (2006). As described in Sect. 3, F11, F46, F51, and F99 appear to be foreground M stars and so are excluded from this compilation; it would appear likely that other interlopers may also be present amongst those stars without current spectral classifications.

Table A.1. continued.

ID	RA (h m s)	Dec (d m s)	m_{F127M} (mag)	m_{F139M} (mag)	m_{F153M} (mag)	m_{F205W} (mag)	#Observations (#Epochs)	Spec. class.	Notes
F47	17 45 50.754	-28 49 25.28	17.02	15.92	14.87	12.90	8(6)	O4-5 Ia	
F48	17 45 50.623	-28 49 26.96	17.69	16.53	15.42	13.28	-	-	
F49	17 45 50.128	-28 49 07.79	17.42	16.25	15.12	12.94	3(3)	O5.5-6 Ia	
F50	17 45 50.134	-28 49 26.17	18.30	17.00	15.77	13.53	6(5)	O4-5 Ia	
F52	17 45 51.206	-28 49 33.31	17.64	16.41	15.24	12.94	-	-	
F53	17 45 50.714	-28 49 25.01	17.11	15.97	14.93	12.94	5(3)	O4-5 Ia	
F54	17 45 50.271	-28 49 15.81	17.93	16.63	15.42	13.02	6(6)	O5.5-6 I-III	
F55	17 45 50.787	-28 49 22.61	17.11	16.02	15.00	13.03	6(5)	O5.5-6 III	
F56	17 45 50.591	-28 49 22.19	17.00	15.92	14.91	13.03	-	-	
F57	17 45 50.768	-28 49 20.31	16.91	-	-	13.04	-	-	
F58	17 45 49.968	-28 49 19.60	17.83	16.57	15.37	13.05	-	-	
F59	17 45 51.138	-28 49 14.34	17.05	15.98	14.95	13.05	-	-	
F60	17 45 50.799	-28 49 22.18	17.21	16.08	15.05	13.02	6(5)	O4-5 Ia	
F61	17 45 50.144	-28 48 59.09	17.38	16.24	15.06	13.09	-	-	
F62	17 45 50.427	-28 49 16.61	17.04	15.99	15.00	13.04	17(14)	O4-5 I-III	
F63	17 45 50.838	-28 49 25.68	17.20	16.15	15.14	13.15	7(6)	O4-5 I-III	
F64	17 45 50.481	-28 49 16.71	17.15	16.10	15.08	13.13	14(10)	O4-5 I-III	
F65	17 45 50.082	-28 49 21.53	17.58	16.42	15.32	13.16	1(1)	O4-5 I-III	Low S/N
F66	17 45 50.532	-28 49 20.42	17.07	15.99	15.00	13.11	-	-	
F67	17 45 50.475	-28 49 15.10	17.69	16.56	15.48	13.35	-	-	
F68	17 45 50.855	-28 49 18.15	16.70	15.68	14.71	12.93	14(11)	O5.5-6 III	
F69	17 45 50.847	-28 49 20.32	17.06	15.99	14.97	13.06	4(4)	O6-6.5 III	
F70	17 45 50.252	-28 49 23.39	17.82	16.59	15.42	13.30	-	-	
F71	17 45 50.060	-28 49 16.43	18.14	16.92	15.77	13.62	-	-	
F72	17 45 50.784	-28 49 20.27	-	16.08	15.05	13.13	-	-	
F73	17 45 50.679	-28 49 25.58	17.78	16.59	15.48	13.35	5(3)	-	Blend
F74	17 45 50.993	-28 49 27.49	17.62	16.50	15.42	13.36	5(5)	O5-6.5 I-III	
F75	17 45 50.825	-28 49 11.25	18.91	17.48	16.05	13.36	-	-	
F76	17 45 50.341	-28 49 17.06	17.64	16.49	15.38	13.38	-	-	
F77	17 45 50.771	-28 49 19.83	17.30	16.26	15.23	13.25	25(10)	O6-6.5 III	
F78	17 45 51.939	-28 49 24.71	17.94	16.77	15.59	13.44	-	-	
F79	17 45 50.074	-28 49 18.11	19.20	17.72	16.23	13.46	-	-	
F80	17 45 50.589	-28 49 19.46	17.40	16.29	15.32	13.47	24(10)	-	Blend
F81	17 45 50.713	-28 49 24.24	17.62	16.51	15.46	13.48	10(5)	O6-7 III-V	
F82	17 45 50.736	-28 49 19.13	17.37	16.30	15.31	13.40	29(10)	O5-6 III-V	
F83	17 45 50.061	-28 49 20.67	18.00	16.81	15.69	13.53	-	-	
F84	17 45 50.526	-28 49 16.28	17.58	16.49	15.61	13.54	18(10)	O6-7 III-V	
F85	17 45 50.484	-28 49 18.60	17.50	16.47	15.46	13.54	17(10)	O7-8 III-V	
F86	17 45 50.985	-28 49 33.59	17.30	16.32	15.35	13.56	-	-	
F87	17 45 50.518	-28 49 16.58	17.62	16.58	15.56	13.60	19(10)	O5-6 V	
F88	17 45 49.653	-28 49 17.23	19.10	17.66	16.22	13.62	-	-	
F89	17 45 50.955	-28 49 17.15	17.33	16.33	15.39	13.65	11(10)	O6-7 V	
F90	17 45 50.570	-28 49 32.97	18.30	17.09	15.94	13.68	5(5)	O5-6 V	Bry infilled
F91	17 45 49.978	-28 49 17.52	18.43	17.19	16.03	13.69	-	-	
F92	17 45 50.518	-28 49 21.45	17.59	16.50	15.44	13.48	12(5)	O5-6 V	Bry infilled
F93	17 45 50.376	-28 49 22.78	18.14	17.04	15.99	13.81	10(8)	O5-6 III-V	Bry infilled
F94	17 45 50.657	-28 49 28.03	18.74	17.50	16.33	14.14	-	-	
F95	17 45 50.578	-28 49 22.00	17.80	16.71	15.69	13.71	-	-	
F96	17 45 50.724	-28 49 19.73	17.36	16.35	15.37	13.54	29(10)	O5-6 III	
F97	17 45 51.385	-28 49 16.57	17.83	16.72	15.67	13.73	-	-	
F98	17 45 51.153	-28 49 37.06	18.08	16.93	15.87	13.75	-	-	
F100	17 45 51.061	-28 49 17.61	17.57	16.55	15.59	13.77	-	-	
F101	17 45 50.914	-28 49 18.37	17.55	16.53	15.58	13.78	14(11)	O6-8 V	
F102	17 45 50.876	-28 49 28.80	18.24	17.07	15.93	13.78	4(4)	O5-8 V	
F103	17 45 49.679	-28 49 22.58	20.16	18.68	17.17	14.53	-	-	
F104	17 45 50.577	-28 49 43.77	18.09	16.96	15.85	13.79	-	-	
F105	17 45 50.596	-28 49 39.60	19.13	17.75	16.37	13.81	-	-	
F106	17 45 49.886	-28 49 23.23	-	-	-	13.82	-	-	
F107	17 45 49.872	-28 49 30.99	18.01	16.89	15.77	13.87	-	-	

Table A.1. continued.

ID	RA (h m s)	Dec (d m s)	m_{F127M} (mag)	m_{F139M} (mag)	m_{F153M} (mag)	m_{F205W} (mag)	#Observations (#Epochs)	Spec. class.	Notes
F108	17 45 50.809	-28 49 10.93	18.12	17.00	15.94	13.89	-	-	
F109	17 45 50.520	-28 49 20.70	18.00	16.91	15.86	13.91	-	-	
F110	17 45 50.574	-28 49 16.35	18.00	16.93	15.90	13.93	18(10)	≥O8 V	
F111	17 45 50.309	-28 49 03.86	18.45	17.25	16.13	13.94	-	-	
F112	17 45 50.507	-28 49 16.36	17.86	16.80	15.81	13.87	14(10)	O6-8 V	
F113	17 45 50.017	-28 49 17.47	18.67	17.42	16.22	13.97	-	-	
F114	17 45 50.804	-28 49 19.07	17.95	16.90	15.90	13.99	22(10)	O6-8 V	
F115	17 45 50.437	-28 49 20.04	17.99	16.91	15.83	13.83	15(10)	O5-6 V	
F116	17 45 50.537	-28 49 06.28	18.77	17.68	16.63	14.01	-	-	
F117	17 45 50.755	-28 49 19.44	18.05	16.99	15.97	14.06	25(10)	O6-8 V	
F118	17 45 50.453	-28 49 25.97	18.66	17.44	16.28	14.08	4(2)	≥O8 V	Low S/N
F119	17 45 50.842	-28 49 22.75	18.18	17.09	16.06	14.06	6(5)	≥O8 V	Low S/N
F120	17 45 50.692	-28 49 29.96	18.75	17.52	16.34	14.09	-	-	
F121	17 45 50.204	-28 49 19.64	18.53	17.35	16.24	14.09	5(5)	≥O8 V	Low S/N
F122	17 45 50.358	-28 49 17.28	18.17	17.09	16.05	14.09	-	-	
F123	17 45 50.685	-28 49 22.35	-	-	-	14.11	-	-	
F124	17 45 50.718	-28 49 17.26	18.48	17.42	16.38	14.11	-	-	
F125	17 45 51.488	-28 49 21.75	19.57	18.12	16.69	14.15	-	-	
F126	17 45 50.930	-28 49 03.63	17.93	16.93	15.98	14.16	-	-	
F127	17 45 51.184	-28 49 31.52	19.45	18.05	16.67	14.16	-	-	
F128	17 45 51.216	-28 49 36.53	18.51	17.37	16.28	14.18	-	-	
F129	17 45 49.529	-28 49 12.72	19.73	18.27	16.82	14.20	-	-	
F130	17 45 50.605	-28 49 27.50	18.80	17.58	16.40	14.21	-	-	
F131	17 45 50.163	-28 49 27.46	19.11	17.80	16.55	14.23	1(1)	≥O8 V	Low S/N
F132	17 45 50.796	-28 49 02.68	18.47	17.34	16.28	14.27	-	-	
F133	17 45 50.771	-28 49 14.97	18.24	17.19	16.19	14.27	-	-	
F134	17 45 50.499	-28 49 36.54	19.21	17.93	16.75	14.28	-	-	
F135	17 45 50.363	-28 49 25.73	18.83	17.61	16.43	14.29	2(2)	≥O8 V	Low S/N
F136	17 45 50.077	-28 49 27.84	19.59	18.18	16.83	14.30	5(5)	O6-8 V	
F137	17 45 51.486	-28 49 21.26	19.94	18.45	16.93	14.32	-	-	
F138	17 45 50.212	-28 49 39.21	19.64	18.24	16.90	14.35	-	-	
F139	17 45 51.207	-28 49 23.41	18.59	17.48	16.33	14.36	1(1)	-	Low S/N
F140	17 45 50.564	-28 49 18.48	18.44	17.38	16.34	14.38	-	-	
F141	17 45 48.827	-28 49 18.81	20.08	18.57	17.06	14.39	-	-	
F142	17 45 50.689	-28 49 24.93	18.63	17.50	16.43	13.41	-	-	
F143	17 45 50.716	-28 49 17.24	-	-	-	14.43	-	-	
F144	17 45 51.526	-28 49 20.58	19.33	18.05	16.79	14.43	-	-	
F145	17 45 51.445	-28 49 20.07	18.45	17.41	16.38	14.44	-	-	
F146	17 45 49.867	-28 49 14.90	18.88	17.70	16.57	14.45	-	-	
F147	17 45 51.354	-28 49 20.00	18.60	17.52	16.47	14.46	-	-	
F148	17 45 51.785	-28 49 28.42	18.69	17.55	16.53	14.47	-	-	
F149	17 45 50.682	-28 49 01.56	19.49	18.20	16.86	14.47	-	-	
F150	17 45 50.456	-28 49 19.64	18.50	17.38	16.34	14.31	18(9)	-	Featureless?
F151	17 45 50.829	-28 49 27.63	18.92	17.75	16.62	14.48	5(5)	-	Featureless
F152	17 45 50.695	-28 49 36.56	19.21	17.96	16.77	14.48	-	-	
F153	17 45 50.360	-28 49 20.00	19.15	17.92	16.74	14.51	8(6)	≥O8 V	Low S/N
F154	17 45 49.992	-28 49 33.20	19.45	18.15	16.89	14.52	-	-	
F155	17 45 50.422	-28 49 19.13	18.65	17.57	16.53	14.52	13(9)	O6-8 V	
F156	17 45 50.642	-28 49 02.15	19.31	18.04	16.76	14.54	-	-	
F157	17 45 50.220	-28 49 24.18	19.11	17.89	16.71	14.55	10(10)	≥O8 V	Low S/N
F158	17 45 51.096	-28 49 21.99	19.09	17.91	16.80	14.56	-	-	
F159	17 45 50.882	-28 49 15.69	19.63	18.49	17.32	14.57	1(1)	-	Low S/N
F160	17 45 50.500	-28 49 15.81	18.61	17.55	16.55	14.59	-	-	
F161	17 45 50.895	-28 49 40.68	19.75	18.43	17.06	14.59	-	-	
F162	17 45 50.820	-28 49 39.10	18.85	17.69	16.56	14.59	-	-	
F163	17 45 50.436	-28 49 23.40	19.84	-	-	14.60	-	-	
F164	17 45 50.862	-28 49 08.47	18.60	17.54	16.54	14.61	-	-	
F165	17 45 51.160	-28 49 15.36	18.60	17.50	16.52	14.65	-	-	
F166	17 45 50.675	-28 49 19.57	18.62	17.57	16.52	14.69	23(9)	-	Blend

Table A.1. continued.

ID	RA (h m s)	Dec (d m s)	m_{F127M} (mag)	m_{F139M} (mag)	m_{F153M} (mag)	m_{F205W} (mag)	#Observations (#Epochs)	Spec. class.	Notes
F167	17 45 50.733	-28 49 17.73	18.24	17.22	16.29	14.42	–	–	
F168	17 45 50.495	-28 49 30.21	19.47	18.21	17.00	14.70	1(1)	–	Low S/N
F169	17 45 50.377	-28 49 20.26	19.13	17.91	16.84	14.72	–	–	
F170	17 45 50.704	-28 49 20.96	18.74	17.67	16.63	14.74	12(5)	–	Blend
F171	17 45 49.275	-28 49 12.13	19.19	18.00	16.86	14.76	–	–	
F172	17 45 50.232	-28 49 17.52	19.05	17.90	16.84	14.76	4(4)	≥O8 V	Low S/N
F173	17 45 50.204	-28 49 20.24	19.10	17.93	16.83	14.80	1(1)	–	Low S/N
F174	17 45 50.745	-28 49 28.20	19.26	18.09	16.95	14.81	3(3)	–	Low S/N
F175	17 45 50.463	-28 49 03.29	19.72	18.44	17.18	14.82	–	–	
F176	17 45 50.283	-28 49 23.85	19.25	18.05	16.94	14.83	3(3)	–	Featureless
F177	17 45 50.604	-28 49 16.87	18.94	17.85	16.81	14.83	12(8)	≥O8 V	Low S/N
F178	17 45 50.824	-28 49 06.95	20.09	18.72	17.32	14.85	–	–	
F179	17 45 51.356	-28 49 21.37	19.53	18.30	17.08	14.85	–	–	
F180	17 45 50.284	-28 48 59.64	19.72	18.43	17.15	14.89	–	–	
F181	17 45 50.567	-28 49 07.70	18.84	17.79	16.79	14.90	–	–	
F182	17 45 50.586	-28 49 22.91	19.00	17.85	16.76	14.70	–	–	
F183	17 45 49.872	-28 49 42.31	20.25	18.83	17.39	14.93	–	–	
F184	17 45 50.008	-28 49 29.43	20.15	18.75	17.40	14.94	3(3)	–	Low S/N
F185	17 45 50.282	-28 49 27.56	19.65	18.40	17.18	14.95	2(2)	≥O8 V	Low S/N
F186	17 45 50.001	-28 49 28.24	20.43	19.01	17.61	14.95	6(6)	≥O8 V	Low S/N
F187	17 45 50.542	-28 49 23.30	19.22	18.10	17.05	14.96	–	–	
F188	17 45 50.936	-28 49 21.80	19.02	17.93	16.91	14.97	2(2)	≥O8 V	Low S/N
F189	17 45 50.595	-28 49 23.52	18.91	17.79	16.69	14.77	3(3)	–	Featureless
F190	17 45 49.759	-28 49 19.76	19.44	18.25	17.14	14.99	–	–	
F191	17 45 51.140	-28 49 18.17	18.83	17.79	16.84	15.00	–	–	
F192	17 45 50.048	-28 49 04.94	19.70	18.43	17.16	15.00	–	–	
F193	17 45 50.383	-28 49 09.56	19.08	17.98	16.93	15.00	–	–	
F194	17 45 50.531	-28 49 07.93	20.41	19.00	17.62	15.01	–	–	
F195	17 45 50.530	-28 49 15.30	19.11	18.00	17.01	15.03	–	–	
F196	17 45 50.463	-28 49 07.74	19.55	18.35	17.18	15.03	–	–	

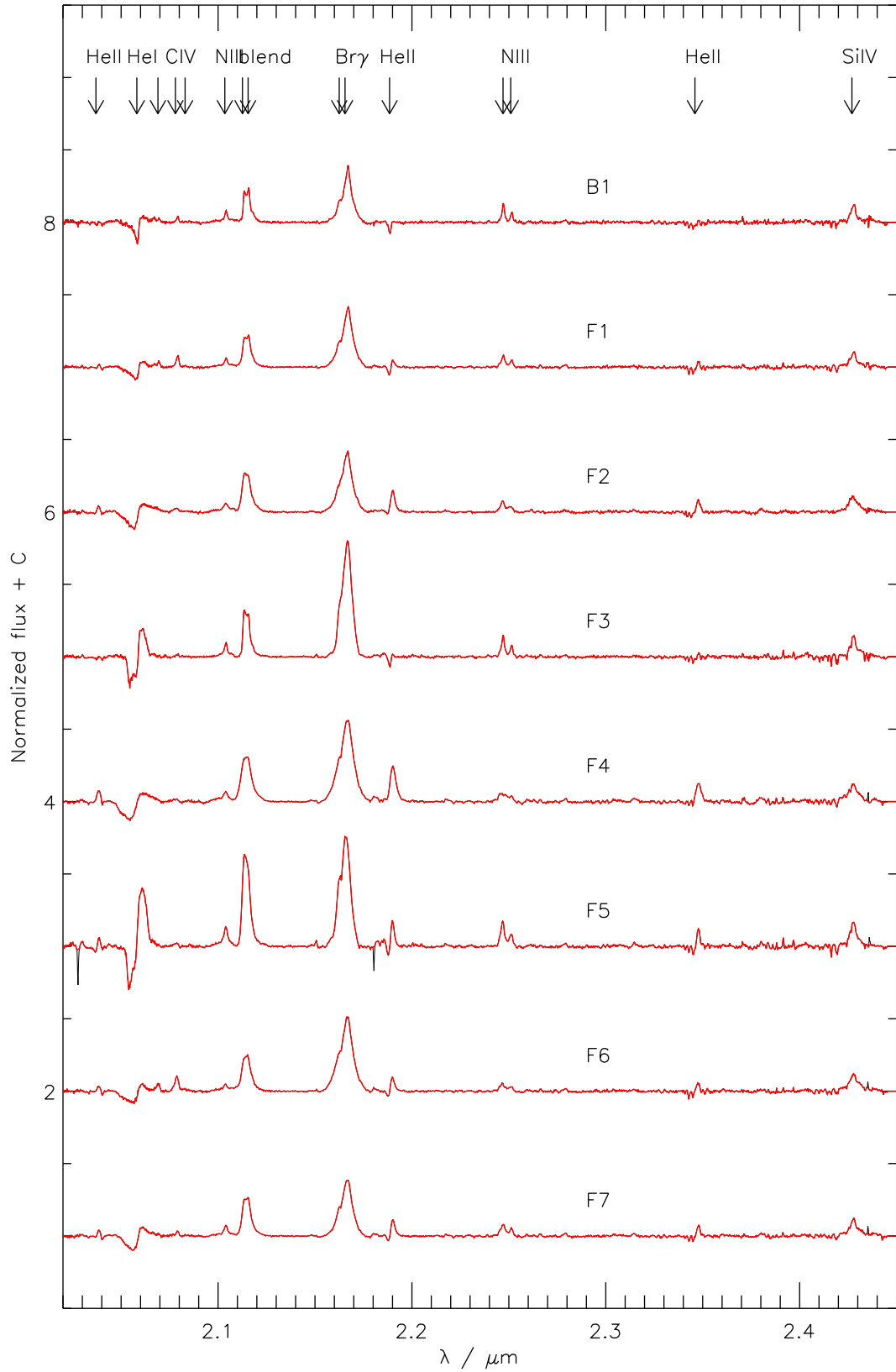


Fig. A.1. Montage of the spectra of all Arches cluster members extracted in this study. We note that spectra corresponding to late spectral type interlopers have been excluded. Black lines correspond to unmodified spectra, red lines reflect spectra that have been manually corrected for spurious features.

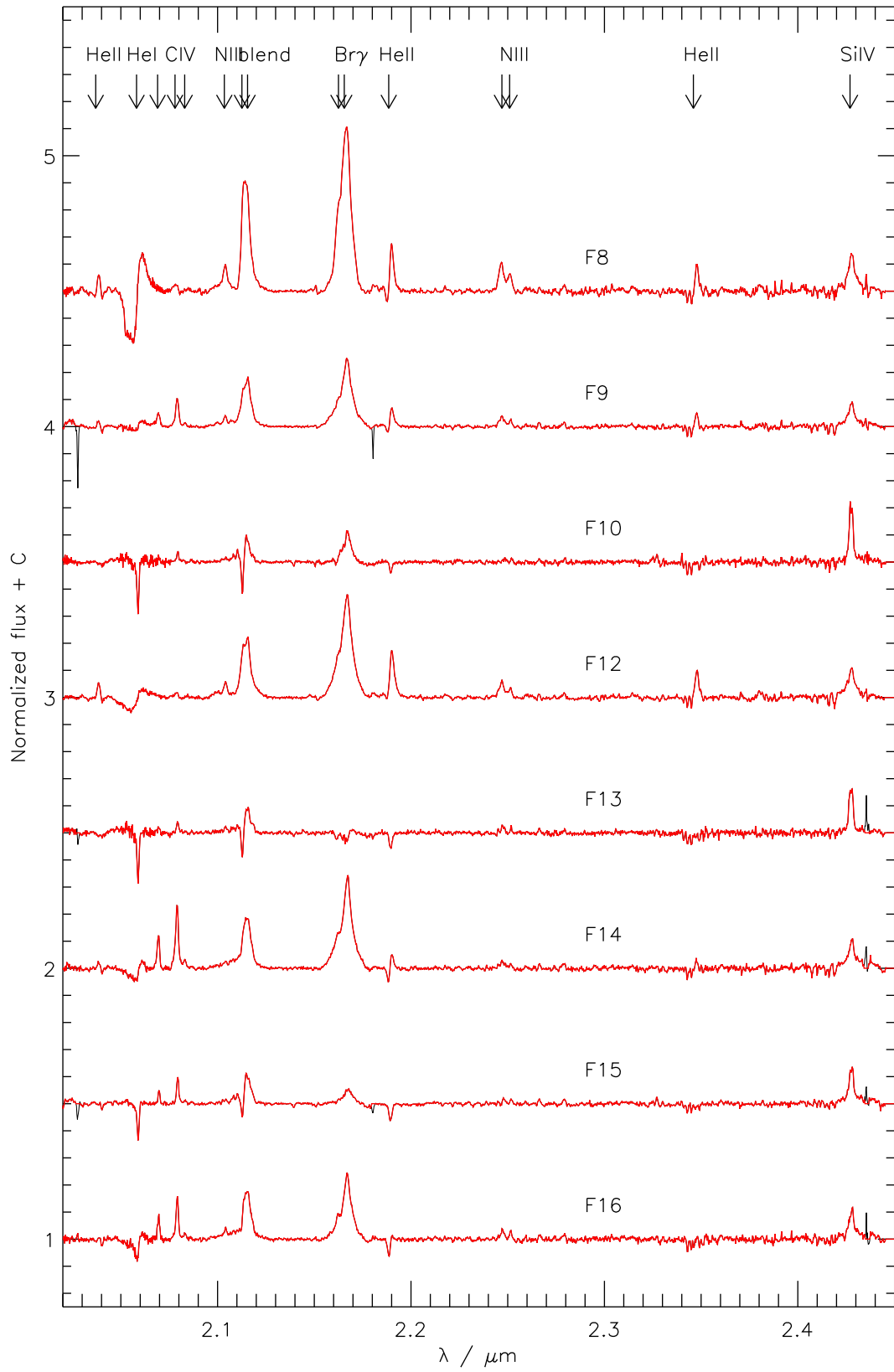


Fig. A.1. continued.

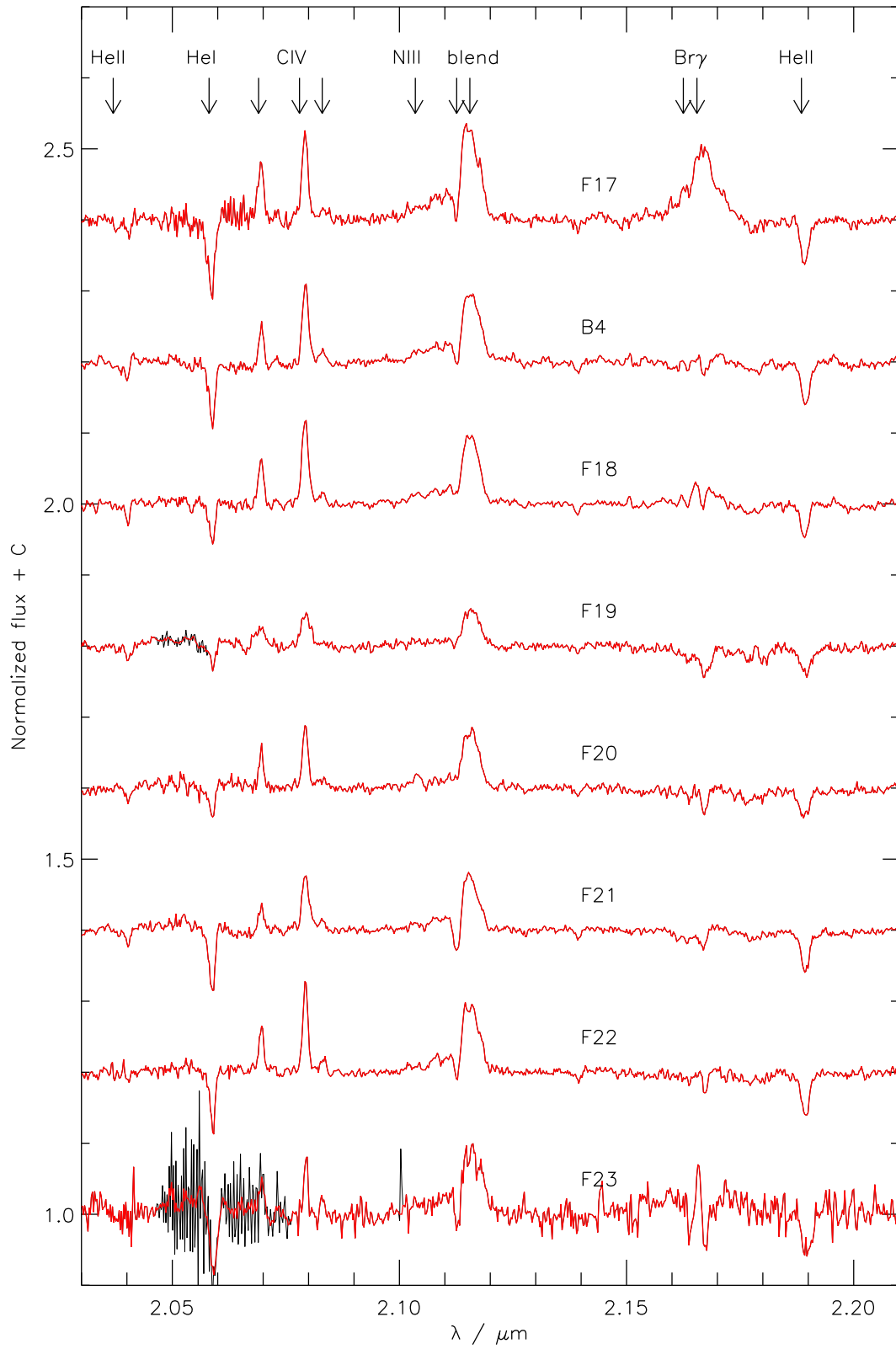


Fig. A.1. continued.

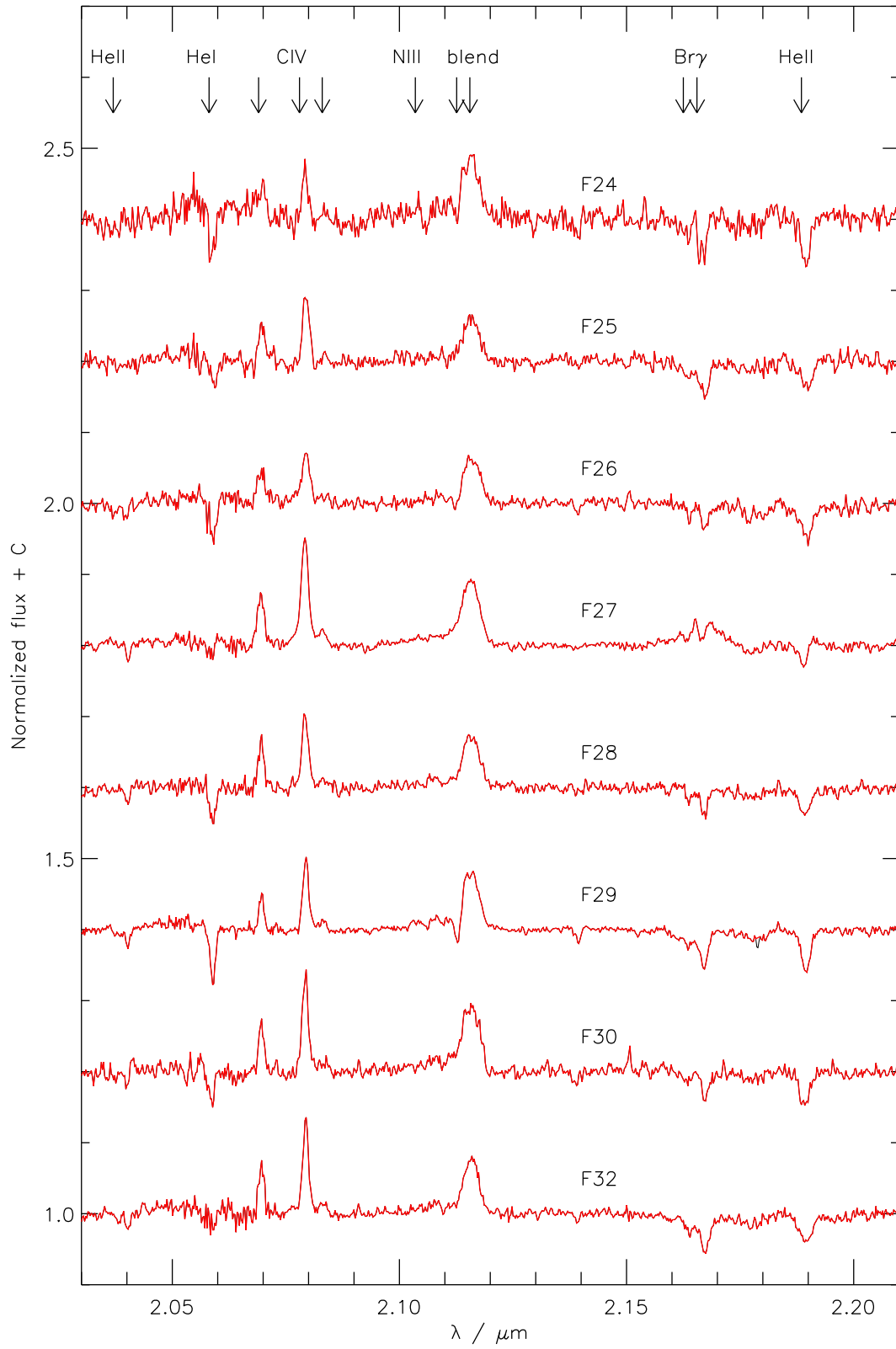


Fig. A.1. continued.

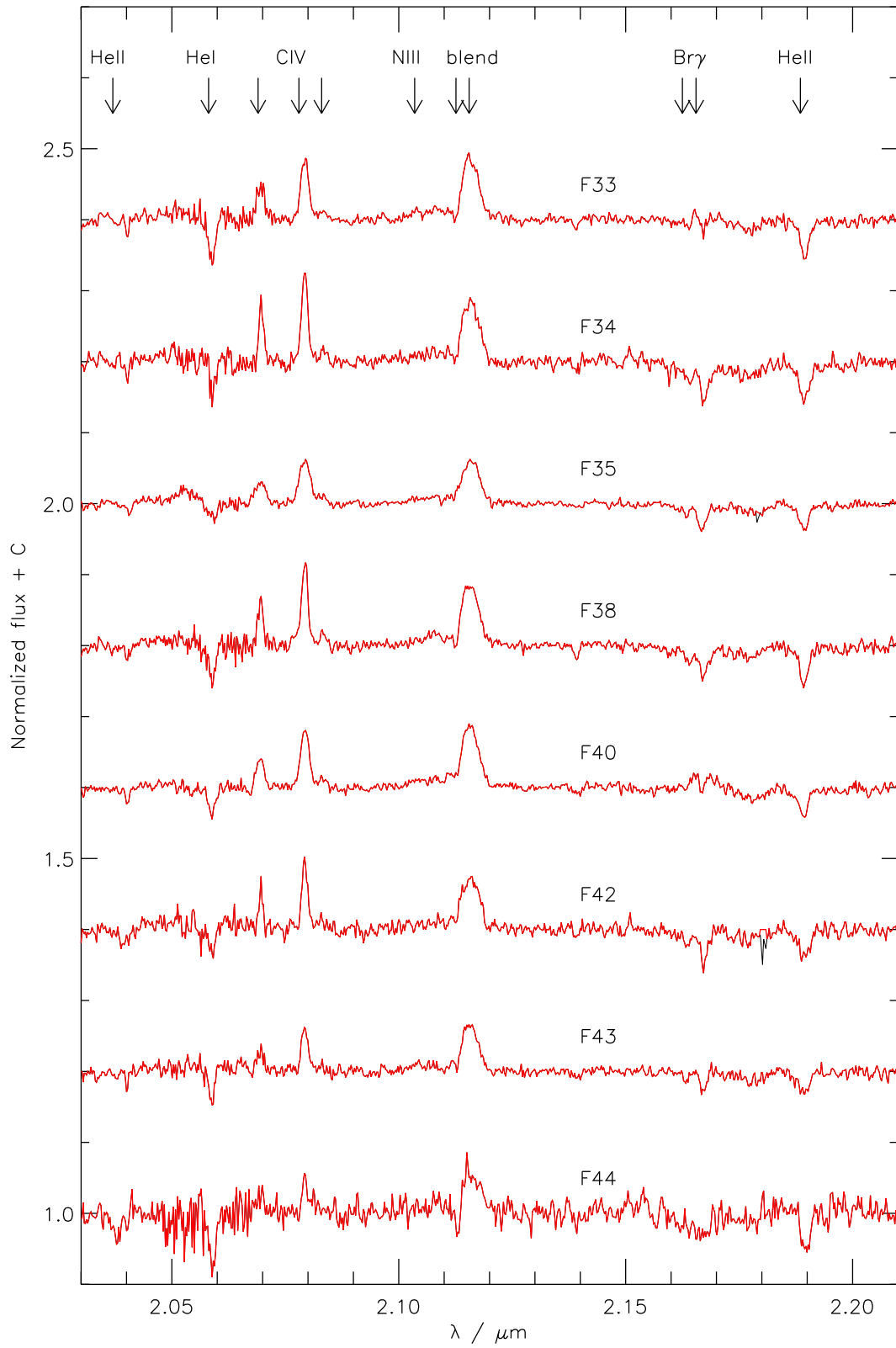


Fig. A.1. continued.

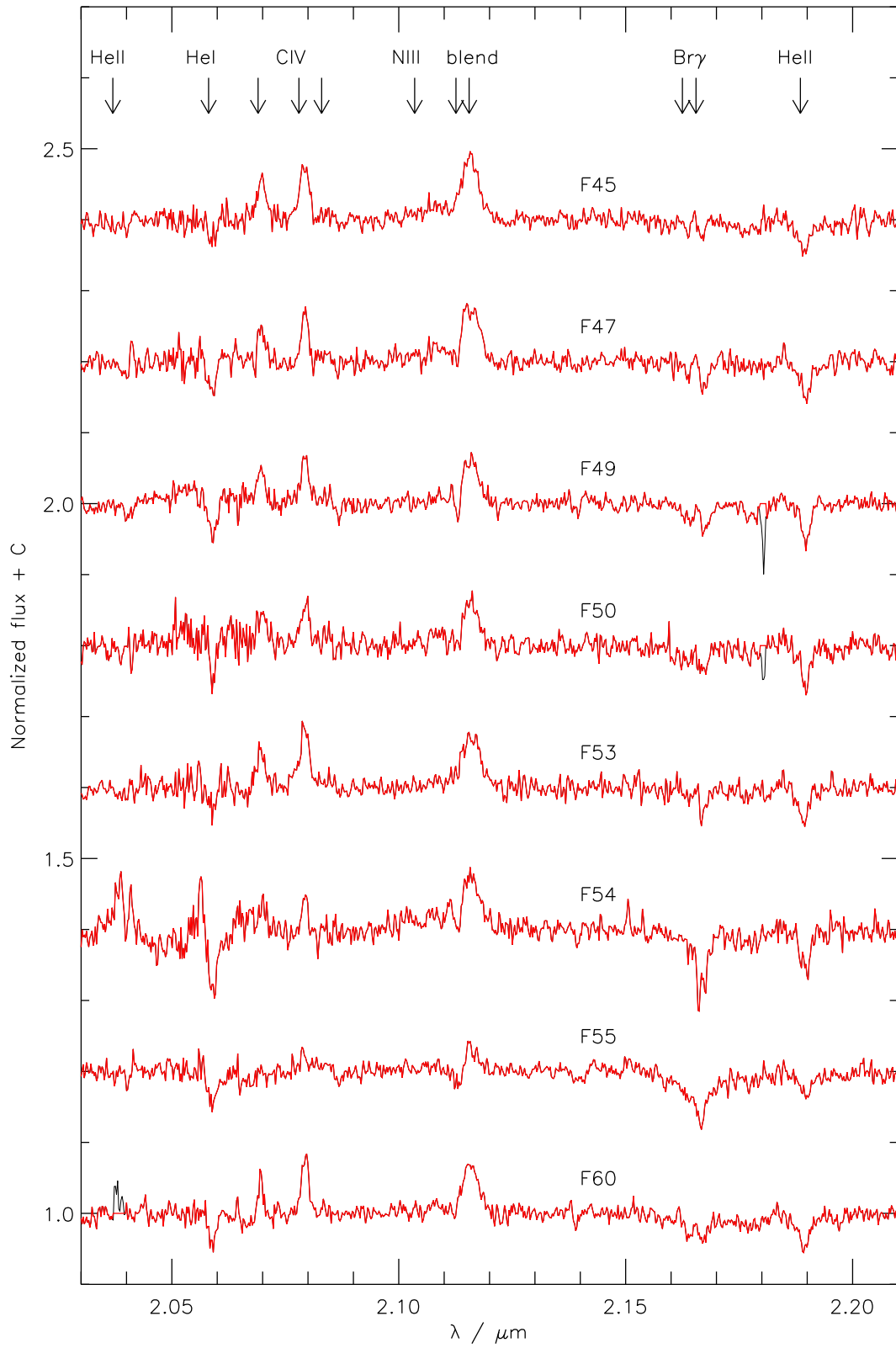


Fig. A.1. continued.

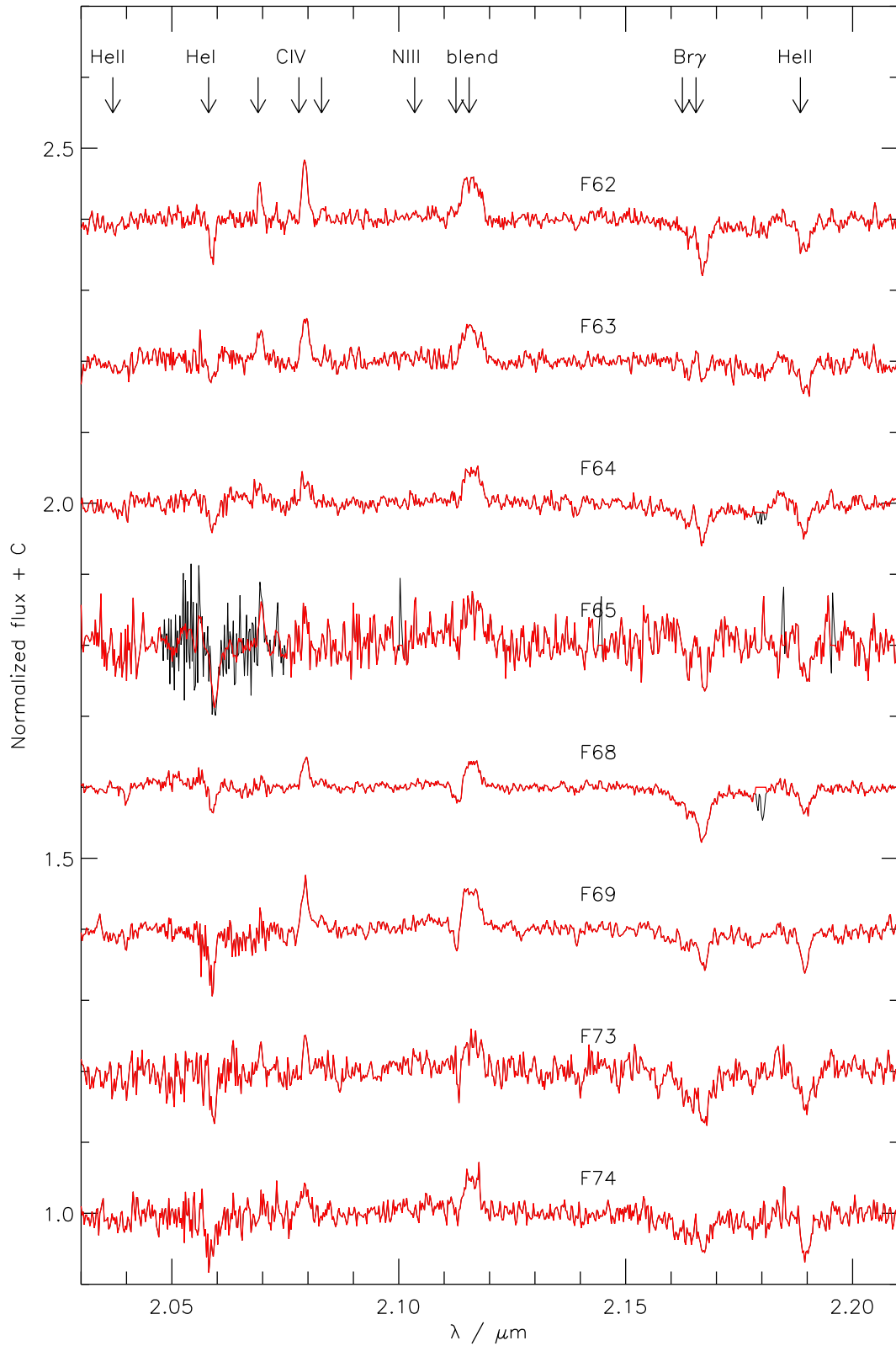


Fig. A.1. continued.

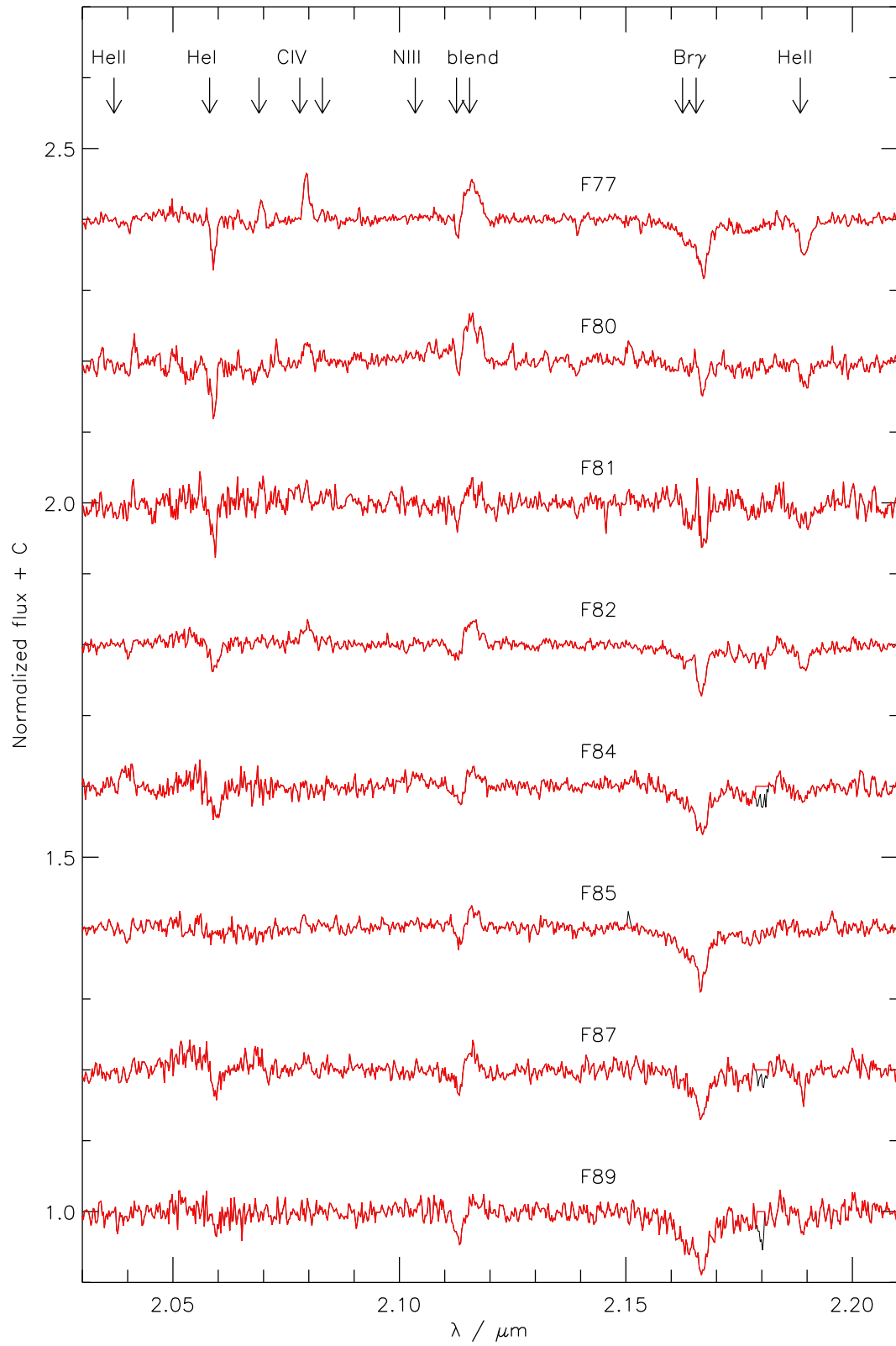


Fig. A.1. continued.

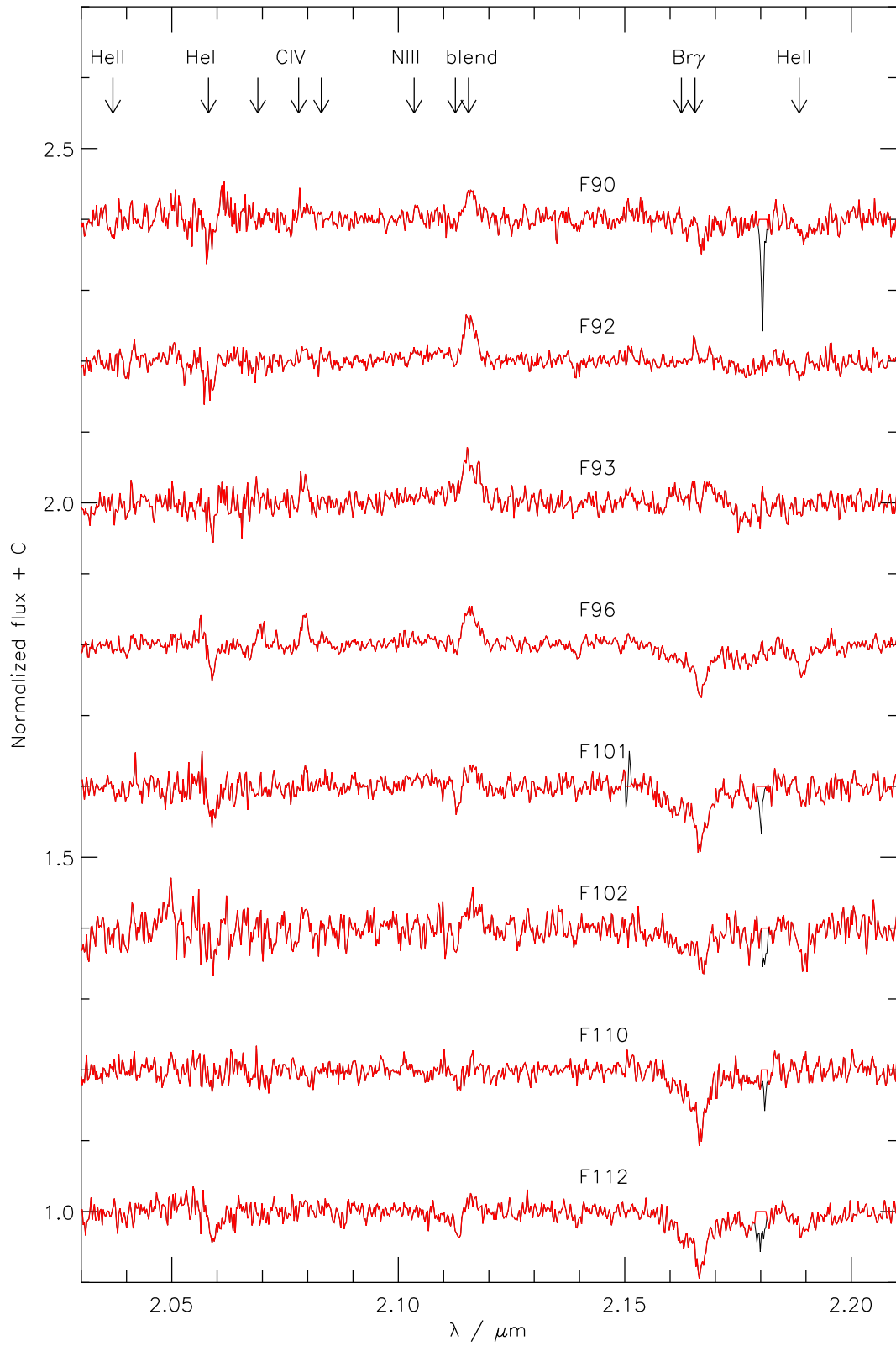


Fig. A.1. continued.

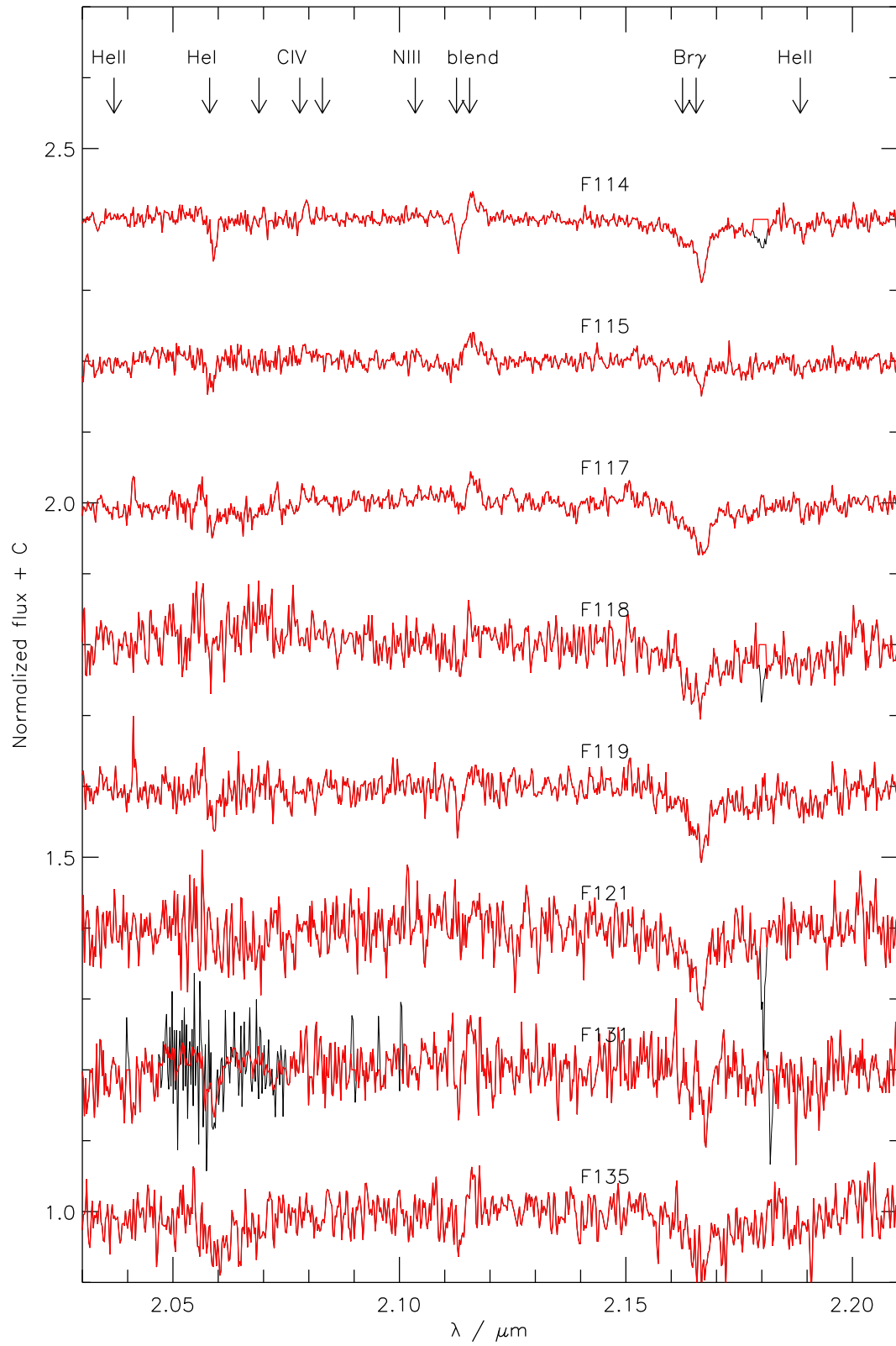


Fig. A.1. continued.

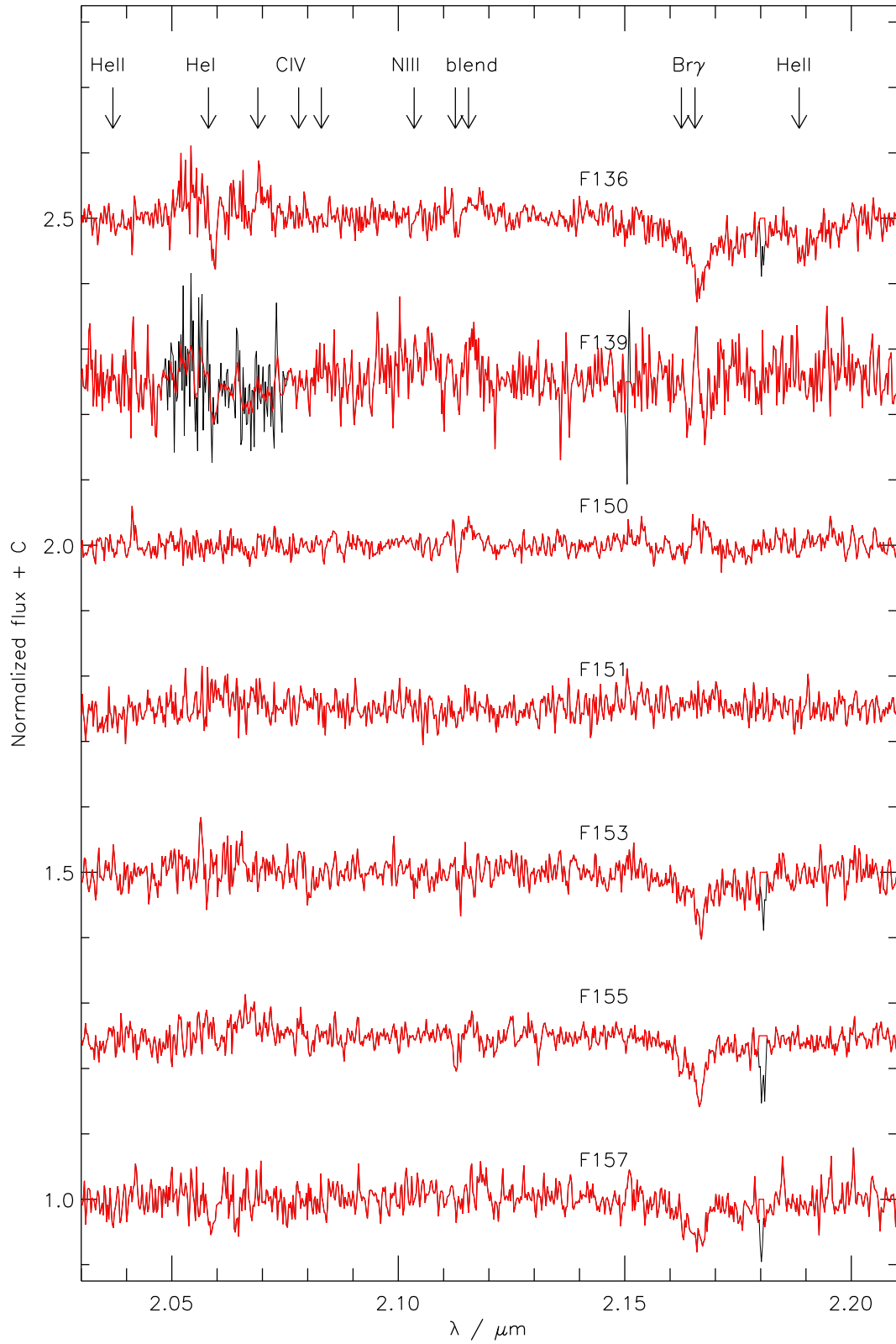


Fig. A.1. continued.

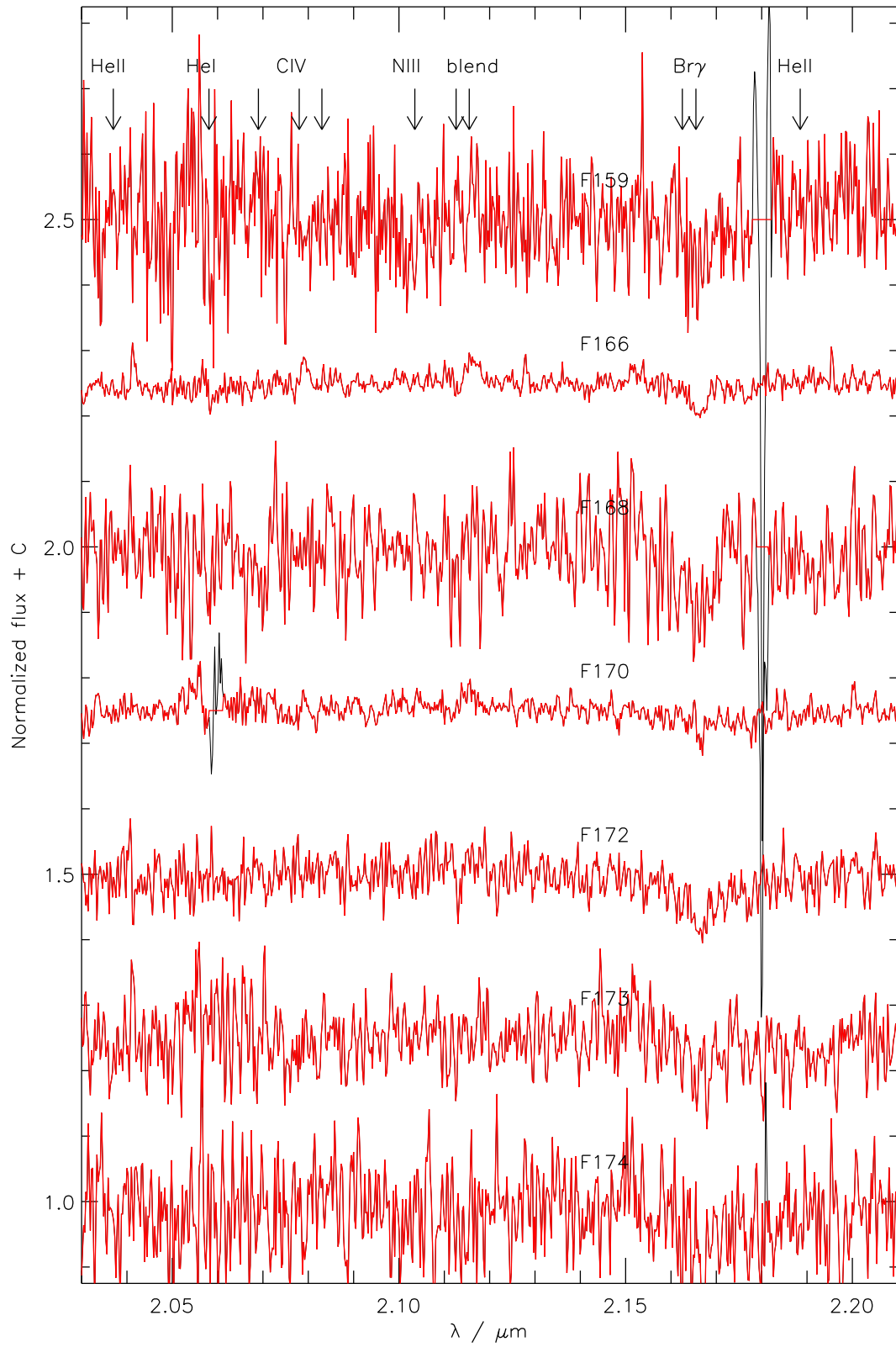


Fig. A.1. continued.

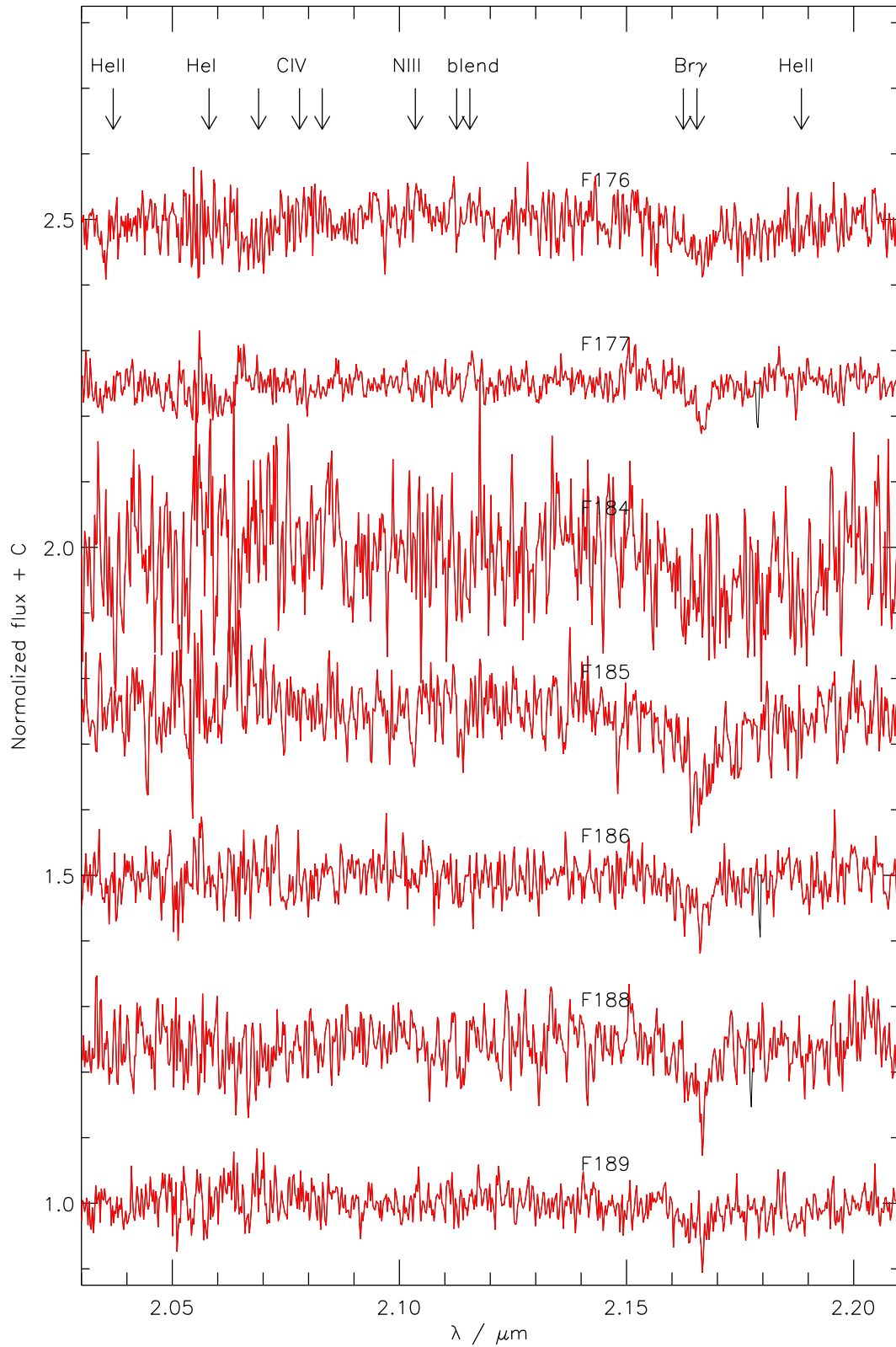


Fig. A.1. continued.

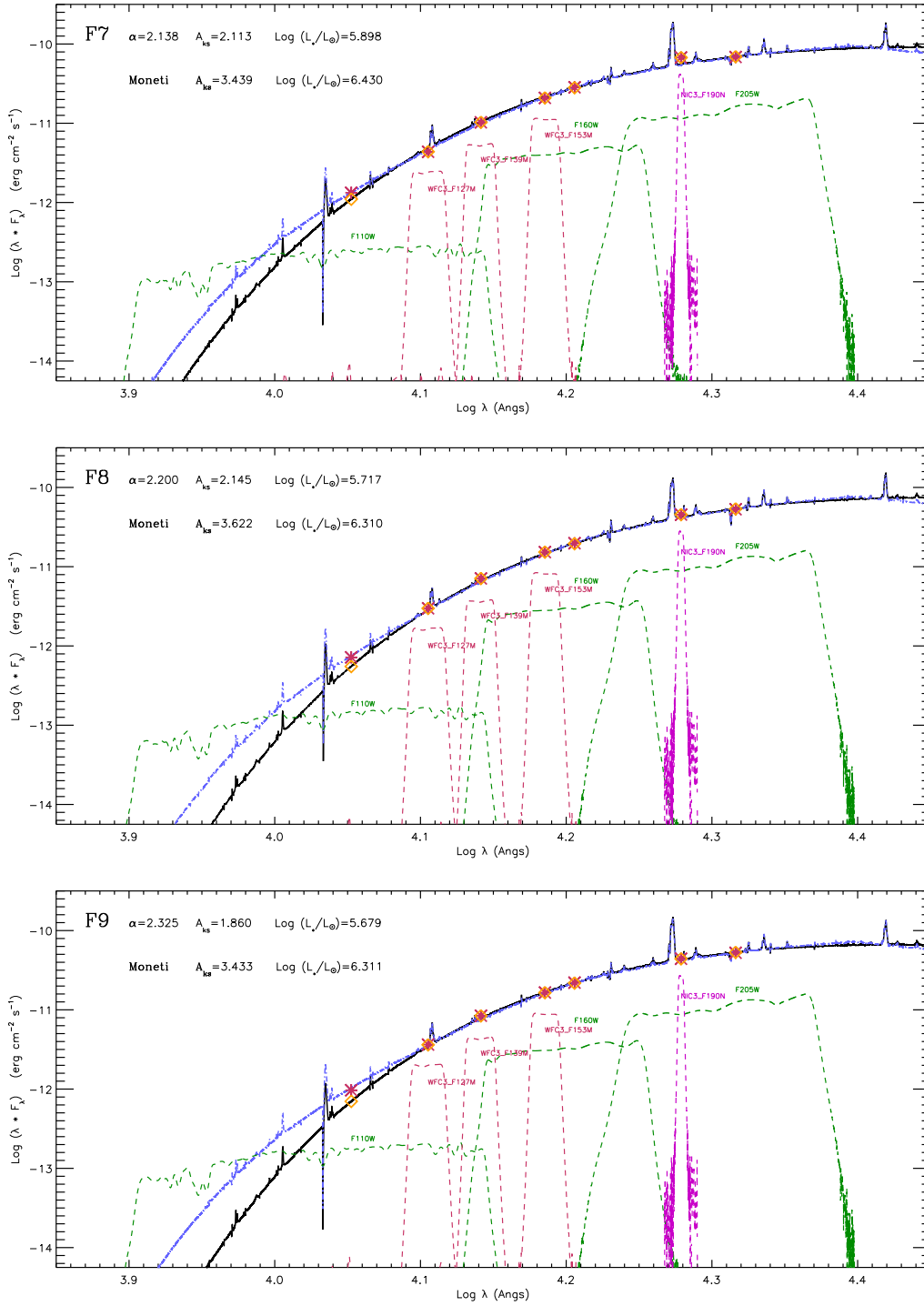


Fig. A.2. Following Fig. 9, synthetic model-atmosphere spectra for the WNLh stars F7, F8, and F9, computed for two differing assumed interstellar reddening laws, illustrating the dramatic dependence of bolometric luminosity on this choice. Photometry employed from Table 1, Fi02, and Dong et al. (2011).